AWARD NUMBER: W81XWH-14-1-0068

TITLE: Defining Translational Reprogramming in Tuberous Sclerosis Complex

PRINCIPAL INVESTIGATOR: Shu-Bing Qian

CONTRACTING ORGANIZATION: Cornell University
Ithaca, NY 14850-2820

REPORT DATE: July 2015

TYPE OF REPORT: Annual Report

PREPARED FOR: U.S. Army Medical Research and Materiel Command
Fort Detrick, Maryland 21702-5012

DISTRIBUTION STATEMENT: Approved for Public Release;
Distribution Unlimited

REPORT DOCUMENTATION PAGE

Form Approved
OMB No. 0704-0188

1. REPORT DATE	2. REPORT TYPE	3. DATES COVERED
July 2015	Annual	07/01/2014 - 06/30/2015

4. TITLE AND SUBTITLE

Defining Translational Reprogramming in Tuberous Sclerosis Complex

5a. CONTRACT NUMBER
W81XWH-14-1-0068

5b. GRANT NUMBER

5c. PROGRAM ELEMENT NUMBER

6. AUTHOR(S)

Shu-Bing Qian

E-Mail: sq38@cornell.edu

5d. PROJECT NUMBER

5e. TASK NUMBER

5f. WORK UNIT NUMBER

7. PERFORMING ORGANIZATION NAME(S) AND ADDRESS(ES)

Cornell University
373 Pine Tree Road
Ithaca, NY 14850

8. PERFORMING ORGANIZATION REPORT NUMBER

9. SPONSORING / MONITORING AGENCY NAME(S) AND ADDRESS(ES)

U.S. Army Medical Research and Materiel Command
Fort Detrick, Maryland 21702-5012

10. SPONSOR/MONITOR'S ACRONYM(S)

11. SPONSOR/MONITOR'S REPORT NUMBER(S)

12. DISTRIBUTION / AVAILABILITY STATEMENT

Approved for Public Release; Distribution Unlimited

13. SUPPLEMENTARY NOTES

14. ABSTRACT

Tuberous sclerosis complex (TSC) is an autosomal dominant disease characterized by benign tumors in various tissues. The genes mutated in this disease, TSC1 and TSC2, encode tumor suppressors that are associated in a complex. The TSC1/2 complex, through its Rheb-GAP activity, is a critical negative regulator of mTORC1 under physiological conditions. Activation of mTORC1 positively stimulates cap-dependent mRNA translation via its downstream substrates S6K and 4E-BP. In our previous study, we demonstrated that TSC-mTORC1 signaling regulates the balance between cap-dependent and cap-independent translation. In this project, we aim to (1) Dissect the molecular linkage between mTORC1 and protein homeostasis; (2) Define the role of mTORC1 in ribosome dynamics and translational re-programming.

15. SUBJECT TERMS
Tuberous sclerosis complex; mTORC1; rapamycin; mRNA; translation; ribosome; quality control; alternative translation

16. SECURITY CLASSIFICATION OF:			17. LIMITATION OF ABSTRACT	18. NUMBER OF PAGES	19a. NAME OF RESPONSIBLE PERSON
a. REPORT	b. ABSTRACT	c. THIS PAGE			USAMRMC
Unclassified	Unclassified	Unclassified	Unclassified	38	19b. TELEPHONE NUMBER *(include area code)*

Table of Contents

Page

1. INTRODUCTION

Tuberous sclerosis complex (TSC) is an autosomal dominant disease characterized by benign tumors in various tissues. The genes mutated in this disease, TSC1 and TSC2, encode tumor suppressors that are associated in a complex. The TSC1/2 complex, through its Rheb-GAP activity, is a critical negative regulator of mTORC1 under physiological conditions. Activation of mTORC1 positively stimulates cap-dependent mRNA translation via its downstream substrates S6K and 4E-BP. In our previous study, we demonstrated that TSC-mTORC1 signaling regulates the balance between cap-dependent and cap-independent translation. In this project, we aim to (1) Dissect the molecular linkage between mTORC1 and protein homeostasis; (2) Define the role of mTORC1 in ribosome dynamics and translational re-programming.

2. KEYWORDS

Tuberous sclerosis complex; mTORC1; rapamycin; mRNA; translation; ribosome; quality control; alternative translation

3. ACCOMPLISHMENTS

- **What were the major goals of the project?**

Task 1. Dissect the Molecular Linkage between mTORC1 and Protein Homeostasis

Task 2. Define the Role of mTORC1 in Ribosome Dynamics and Translational Re-programming

- **What was accomplished under these goals?**

1. TISdb: a database for alternative translation initiation in mammalian cells.

Proper selection of the translation initiation site (TIS) on mRNAs is crucial for the production of desired protein products. Recent studies using ribosome profiling technology uncovered a surprising variety of potential TIS sites in addition to the annotated start codon. The prevailing alternative translation reshapes the landscape of proteome in terms of diversity and complexity. To identify the hidden coding potential of transcriptome in mammalian cells, we developed global translation initiation sequencing (GTI-Seq) that maps genome-wide TIS positions at nearly single nucleotide resolution. To facilitate studies of alternative translation, we created a database of alternative TIS sites identified from human and mouse cell lines based on multiple GTI-Seq replicates. The TISdb, available at http://tisdb.human.cornell.edu, includes 6,991 TIS sites from 4,961 human genes and 9,973 TIS sites from 5,668 mouse genes. The TISdb website provides a simple browser interface for query of high-confidence TIS sites and their associated open reading frames (ORFs). The output of search results provides a user-friendly visualization of TIS information in the context of transcript isoforms. Together, the information in the database provides an easy reference for alternative translation in mammalian cells and will support future investigation of novel translational products.

2. Ribosome profiling reveals sequence-independent post-initiation pausing as a signature of translation.

The journey of a newly synthesized polypeptide starts in the peptidyltransferase center of the ribosome, from where it traverses the exit tunnel. The interior of the ribosome exit tunnel is neither straight nor smooth. How the ribosome dynamics in vivo is influenced by the exit tunnel is poorly understood. Genome-wide ribosome profiling in mammalian cells reveals elevated ribosome density at the start codon and surprisingly the downstream 5th codon position as well (Fig. 1). We found that the highly focused ribosomal pausing shortly after initiation is attributed to the geometry of the exit tunnel, as deletion of the loop region from ribosome protein L4 diminishes translational pausing at the 5th codon position. Unexpectedly, the ribosome variant undergoes translational abandonment shortly after initiation, suggesting that there exists an obligatory step between initiation and elongation commitment. We propose that the post-initiation pausing of

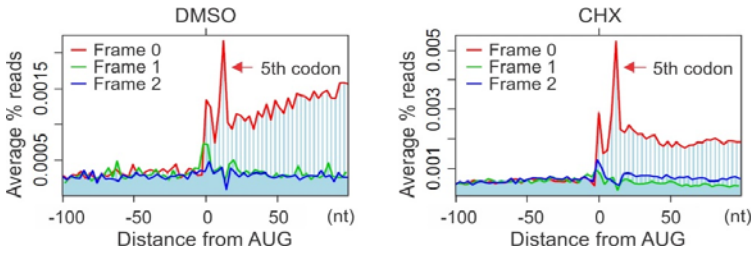

Fig. 1. Metagene analysis of RPFs obtained from HEK293 cells treated with CHX (right) or DMSO control (left).

ribosomes represents an inherent signature of the translation machinery to ensure productive translation.

3. Quantitative profiling of initiating ribosomes *in vivo*.

Cells have evolved exquisite mechanisms to fine-tune the rate of protein synthesis in response to stress. Systemic mapping of start-codon positions and precise measurement of the corresponding initiation rate would transform our understanding of translational control. Here we present quantitative translation initiation sequencing (QTI-seq), with which the initiating ribosomes can be profiled in real time at single-nucleotide resolution (Fig. 2). Resultant initiation maps not only delineated variations of start-codon selection but also highlighted a dynamic range of initiation rates in response to nutrient starvation. The integrated data set provided unique insights into principles of alternative translation and mechanisms controlling different aspects of translation initiation. With RiboTag mice, QTI-seq permitted tissue-specific profiling of initiating ribosomes in vivo. Liver cell-specific ribosome profiling uncovered a robust translational reprogramming of the proteasome system in fasted mice. Our findings illuminated the prevalence and dynamic nature of translational regulation pivotal to physiological adaptation in vivo.

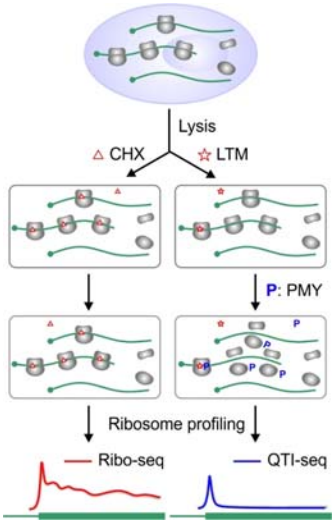

Fig. 2. Schematic of Ribo-seq (left) and QTI-seq (right) procedures.

4. Translational control of cytosolic stress response by mitochondrial ribosomal protein L18.

In response to stress, cells attenuate global protein synthesis but permit efficient translation of mRNAs encoding heat shock proteins (HSPs). Despite decades since the first description of the heat shock response, how cells achieve translational control of HSP synthesis remains enigmatic. Here we report an unexpected role for mitochondrial ribosomal protein L18 (MRPL18) in mammalian cytosolic stress response. MRPL18 bears a downstream CUG start codon and generates a cytosolic isoform in a stress-dependent manner. The cytosolic MRPL18 incorporates into the 80S ribosome and facilitates ribosome engagement on mRNAs selected for translation during stress. MRPL18 knockdown has minimal effects on mitochondria function, but substantially dampens cytosolic HSP expression at the level of translation. Our results uncover a hitherto uncharacterized stress adaptation mechanism in mammalian cells, which involves formation of a “hybrid” ribosome responsible for translational regulation of cytosolic stress response (Fig. 3).

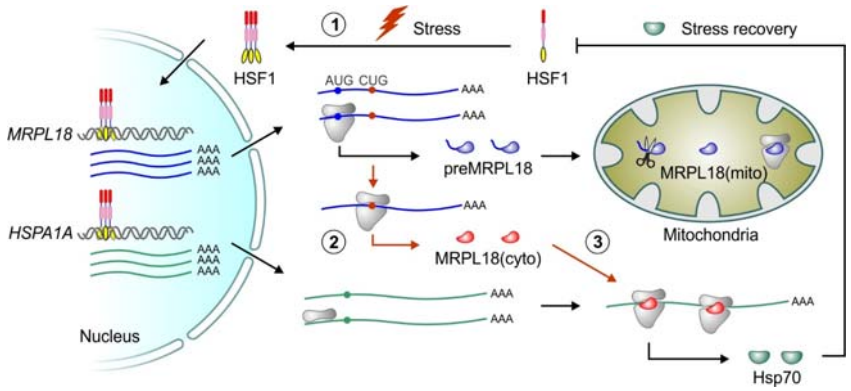

Fig. 3. A model for MRPL18 in translational control during stress conditions. In stressed cells, MRPL18 undergoes alternative translation from the downstream CUG start codon, which results in a cytoplasmic isoform of MRPL18 (red) (2). MRPL18(cyto) incorporates into the 80S ribosome complex, facilitating the engagement of mRNAs highly expressed under stress, such as *Hspa1a* (green) (3).

- **What opportunities for training and professional development has the project provided?**

Nothing to report

- **How were the results disseminated to communities of interest?**

Nothing to report

- **What do you plan to do during the next reporting period to accomplish the goals?**

1. Elucidating the role of mRNA modification in translational control

N6-methyladenosine (m6A) is a ubiquitous modification in mRNA and other RNAs across most eukaryotes. For many years, however, the exact functions of m6A were mot clearly understood. The discovery that the fat mass and obesity-associated protein (FTO) is an m6A demethylase indicates that this modification is reversible and dynamically regulated. Recent m6A profiling in mouse and human cells further showed that this modification is a widespread mark in coding and noncoding RNA transcripts. It is likely that, reversible RNA methylation, analogous to reversible DNA and histone modifications, may affect gene expression. In collaborating with Samie Jeffery's lab at Cornell Weill Medical School, we are investigating the role of m6A modification in translation control. Our preliminary results indicate that stress-inducible Hsp70 translation is regulated by m6A modification. By coupling m6A profiling with QTI-seq, we aim to elucidate the mechanism underlying m6A modification-mediated translational control.

2. Linking mitochondrial tRNA modification and the proteome landscape

Mitochondrion represents an elegant example of a self-sustained system. Bearing its own genome and the translation machinery, mitochondria produces proteins necessary for ATP production. Approximately 200 pathogenic mutations have been mapped to mitochondrial tRNA (mt tRNA) genes. Chemical modifications are a characteristic structural feature of mt tRNAs which contain 16 species of modified nucleosides including three that are mitochondria-specific. Loss of modifications found at the wobble positions of mt tRNAs have been implicated in disrupted tRNA structures that may affect their translation capability. However it is still not completely understood how mt tRNA modification contributes to the regulation of the mitochondrial proteome. In particular, there is little mechanistic knowledge about the nature of crosstalk between mitochondrial activity and cellular stress signals.

To address this complex biological problem in a systematic manner, we developed innovative approaches by coupling high-resolution ribosome profiling with quantitative mapping of tRNA modification. Mridu Saikia, the new postdoc in my laboratory, hypothesized that mt tRNA modification acts as a sentinel for cellular stress signals and the altered proteome triggers mitonuclear protein imbalance and contributes to disease development. We will determine how cellular stress affects mitochondrial metabolism, map mt tRNA modification in response to stress, and define the role of mt tRNA modification in translation.

4. IMPACT

- **What was the impact on the development of the principal discipline(s) of the project?**

To maintain protein homeostasis, cells have evolved several highly coordinated systems to sense and respond to environmental cues. Coupling with the chaperone network, autophagy, and ubiquitin/proteasome system, translation lies at the heart of protein homeostasis. Translational re-programming allows selective translation of mRNAs to maintain the expression of specific proteins during patho-physiological conditions. Such regulation can be quantitative (all-or-none vs. graded), qualitative (enabling a single mRNA to produce several different proteins), or selective (activating subsets of mRNAs for translation). We developed quantitative profiling of initiating ribosomes that permits high resolution mapping of alternative translation initiation sites. Our study reveals that translational re-programming plays a crucial role in cellular metabolism.

- **What was the impact on other disciplines?**

Nothing to report

- **What was the impact on technology transfer?**

Nothing to report

- **What was the impact on society beyond science and technology?**

Nothing to report

5. CHANGES / PROBLEMS

Nothing to report

6. PRODUCTS

- **Publications, conference papers, and presentations**

Journal publications (* Corresponding author)

1. Gao X, Wan J, and Qian SB*. Genome-wide profiling of alternative translation initiation sites. ***Methods Mol Biol*** 2015 (in press)
2. Zhang X, Gao X, Roots RA, Conn CS, Liu B, and Qian SB*. Translational control of cytosolic stress proteins by mitochondrial ribosomal protein L18. ***Nat Struct Mol Biol*** 2015; 22(5):404-10
3. Gao X, Wan J, Liu B, Ma M, Shen B, and Qian SB*. Quantitative profiling of initiating ribosomes in vivo. ***Nat Methods*** 2015; 12(2):147-53
4. Han Y, Gao X, Liu B, Wan J, Zhang X, and Qian SB*. Ribosome profiling reveals sequence-independent post-initiation pausing as a signature of translation. ***Cell Res*** 2014; 24(7):842-51
5. Liu B and Qian SB*. Invited review: Mechanisms of translational regulation during stress. ***Wiley Interdiscip Rev RNA*** 2014; 5(3):301-5
6. Wan J and Qian SB*. TISdb: a database for alternative translation initiation in mammalian cells. ***Nucleic Acids Res*** 2014; 42(1):D845-50

Acknowledgement of federal support: Yes.

- **Other products**

Databases: http://tisdb.human.cornell.edu

TISdb: a database for alternative translation initiation in mammalian cells.

7. PARTICIPANTS & OTHER COLLABORATING ORGANIZATIONS

- **What individuals have worked on the project?**

Name: Shu-Bing Qian, PhD
Project Role: PI
Nearest person month worked: 1
Contribution to Project: Dr. Qian is responsible for the overall administration and direction of the project, including designing experimental protocols, interpreting results, writing manuscripts and supervising research assistants.

Name: Jun Zhou, PhD
Project Role: Postdoc
Nearest person month worked: 12
Contribution to Project: Dr. Zhou will be responsible for ribosome profiling experiments (Aim 1, Aim 2).

- **Has there been a change in the active other support of the PD/PI(s) or senior/key personnel since the last reporting period?**

Nothing to report

- **What other organizations were involved as partners?**

Nothing to report

8. SPECIAL REPORTING REQUIREMENTS

N/A

9. APPENDICES

Copies of journal articles

Cell Research (2014) 24:842-851.

www.nature.com/cr

ORIGINAL ARTICLE

Ribosome profiling reveals sequence-independent post-initiation pausing as a signature of translation

Yan Han[1, 2, *], Xiangwei Gao[1, *], Botao Liu[3], Ji Wan[1], Xingqian Zhang[1], Shu-Bing Qian[1, 3]

[1]Division of Nutritional Sciences, Cornell University, Ithaca, NY 14853, USA; [2]Department of Infectious Diseases, Ruijin Hospital, Shanghai Jiaotong University School of Medicine, Shanghai 200025, China; [3]Graduate Field of Genetics, Genomics and Development, Cornell University, Ithaca, NY 14853, USA

The journey of a newly synthesized polypeptide starts in the peptidyltransferase center of the ribosome, from where it traverses the exit tunnel. The interior of the ribosome exit tunnel is neither straight nor smooth. How the ribosome dynamics *in vivo* is influenced by the exit tunnel is poorly understood. Genome-wide ribosome profiling in mammalian cells reveals elevated ribosome density at the start codon and surprisingly the downstream 5th codon position as well. We found that the highly focused ribosomal pausing shortly after initiation is attributed to the geometry of the exit tunnel, as deletion of the loop region from ribosome protein L4 diminishes translational pausing at the 5th codon position. Unexpectedly, the ribosome variant undergoes translational abandonment shortly after initiation, suggesting that there exists an obligatory step between initiation and elongation commitment. We propose that the post-initiation pausing of ribosomes represents an inherent signature of the translation machinery to ensure productive translation.

***Keywords*:** ribosome; translation

Cell Research (2014) **24**:842-851. doi:10.1038/cr.2014.74; published online 6 June 2014

Introduction

Ribosomes decode the genetic information in mRNA and convert it into the amino acid sequences of proteins. During mRNA translation, the ribosome does not proceed at a constant rate but rather in a stop-and-go movement manner [1]. Variations of elongation speed may result from local stable mRNA structures [2], the presence of rare codons [3], or the interactions between the nascent chain and the ribosome and/or exogenous factors [4]. Frequent translational pausing may have functional importance for the cellular production line. For instance, ribosome stalling could trigger frame-shifting or translational abandonment [5, 6]. A growing body of evidence suggests that cells purposely employ ribosomal pausing as a regulatory mechanism to maintain intracellular protein homeostasis. For example, translational delays in specific regions facilitate co-translational folding of nascent chains [7]. Ribosomes also adopt early elongation pausing in response to various stress conditions [8, 9]. Given the wide range of impacts of ribosome pausing on cellular systems, a fundamental question is to dissect the mechanistic basis underlying translational pausing and determine the physiological consequences when ribosomes stall on individual mRNAs.

Despite several decades since the first description of ribosome pausing and stacking during translation [10], it was not possible until now to measure ribosome dynamics *in vivo* at the genome-wide scale. Ribosome profiling or Ribo-seq, based on deep sequencing of ribosome-protected mRNA fragments (RPFs), has proven to be powerful in determining ribosome positions and densities across the entire transcriptome [11]. Many research groups have successfully applied Ribo-seq to a wide range of organismal species and reported pervasive pause sites along the coding region (CDS) of mRNAs [12-18]. From bacteria to human cells, the most consistent pause

*These two authors contributed equally to this work.
Correspondence: Shu-Bing Qian
E-mail: sq38@cornell.edu
Received 12 February 2014; revised 30 March 2014; accepted 24 April 2014; published online 6 June 2014

sites are located at the start and stop codons, which is in line with the notion that ribosomes tend to pause during initiation and termination [10]. Ribosome profiling also captures many sequence-dependent stalling sites [15]. However, much less is known about translational pausing governed by factors other than *cis*-elements.

Here, we report and characterize a specific ribosomal pausing at the 5th codon position of mRNA CDSs in mammalian cells. Unlike sequence-dependent elongation pausing, the ribosome stalling shortly after initiation is attributed to the geometry of the exit tunnel. Importantly, modifying the exit tunnel not only reduces the ribosomal pausing at the 5th codon position, but results in an unexpected translational abandonment. Our finding suggests a rich communication between the nascent chain and the translation machinery in regulating ribosome kinetics during translation.

Results

Ribosome profiling reveals post-initiation pausing

We applied a modified Ribo-seq to HEK293 cells and examined the average pattern of ribosome density across the entire transcriptome [8, 19]. As expected, the mapped RPF reads start an abrupt accumulation at the annotated start codon [11] (Figure 1A). Interestingly, we observed another prominent peak at the 12 nt downstream position, corresponding to the 5th codon position of the CDS (Figure 1A, red arrow). This is not due to cycloheximide (CHX)-mediated translational arrest because the same feature is maintained in cells without any drug treatment (Figure 1A, left panel). The ribosomal pausing at the

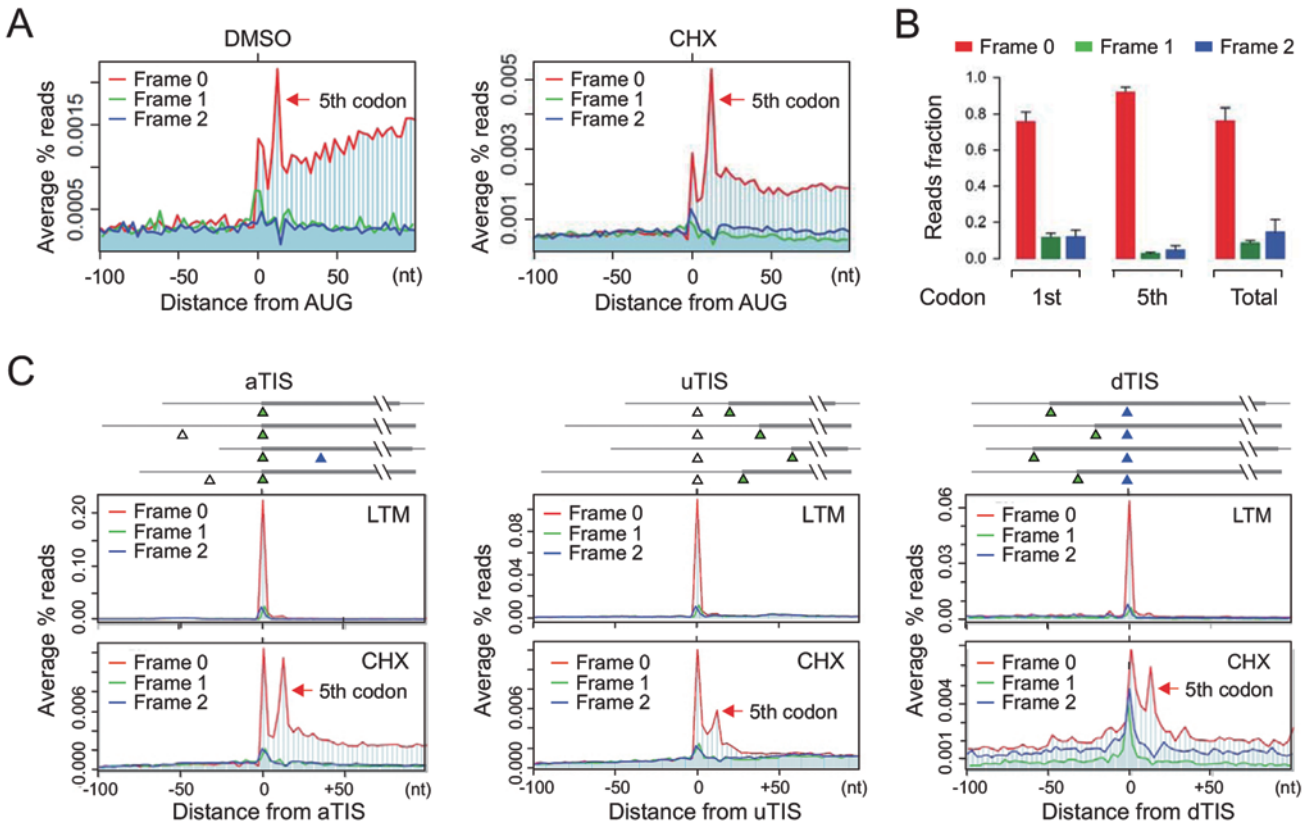

Figure 1 Characterization of post-initiation pausing. **(A)** Metagene analysis of RPFs obtained from HEK293 cells treated with CHX (right) or DMSO control (left). All mapped reads are aligned at the annotated start codon AUG and stratified by frames. The read density at each nucleotide position is averaged using the P-site of RPFs. The red arrow indicates the 5th codon position. **(B)** Read fractions relative to the annotated reading frame are calculated for RPFs mapped to the 1st (AUG) codon, 5th codon, or the entire CDS. Data are shown as means ± SD, $n = 4$. **(C)** Metagene analysis of RPFs obtained from HEK293 cells treated with LTM (upper) or CHX (bottom). All mapped reads are aligned at the annotated start codon (aTIS, green triangle; left panel), upstream TIS (uTIS, white triangle; middle panel), or downstream TIS (dTIS, blue triangle; right panel). The read density at each nucleotide position is averaged using the P-site of RPFs. The red arrow indicates the 5th codon position.

5th codon position is highly reproducible as evidenced by the similar pattern of RPF distribution in a total of 4 independent biological replicates (Supplementary information, Figure S1). To confirm whether the same feature also exists in different cell types, we conducted Ribo-seq in HeLa cells and a mouse embryonic fibroblast (MEF) cell line. Both cells showed consistent pattern of RPFs with prominent peaks of ribosome density at both the start codon and the 5th codon position (Supplementary information, Figure S2). Thus, the excess of ribosome density at the 5th codon position represents a strong ribosomal pausing shortly after initiation.

The post-initiation pausing bears several unique features that distinguish it from the typical ribosome pausing at the start codon. First, the RPFs recovered at the 5th codon position demonstrate a near perfect framing or phasing with > 90% of reads mapped to the same frame as the annotated ORFs (Figure 1A and 1B). This is in contrast to the RPF reads derived from other CDS regions including the AUG start codon, in which about a quarter of the reads are out of the annotated reading frame (Figure 1B). Second, RPFs derived from the 5th codon position have different size distribution in length (Supplementary information, Figure S3). While the majority of footprints mapped to the entire CDS were 29-mer, a substantial proportion of RPFs mapped to the 5th codon position are 27-mer. These results suggest that the stalled ribosome at the 5th codon position might adopt a more compact conformation than the others. Supporting this notion, recent studies demonstrated that the length of footprints could be influenced by ribosome dynamics [20, 21].

To rule out the possibility that the prominent ribosomal pausing at the 5th codon position is due to reinitiation, we segregated initiating ribosomes from elongating ribosomes by applying a translation inhibitor lactimidomycin (LTM). Unlike CHX that freezes all the ribosomes engaged on mRNAs, LTM preferentially acts on the initiating ribosome but not the elongating one [22]. As we reported previously, LTM-based ribosome profiling (GTI-seq) offers global mapping of translation initiation sites (TIS) at single-nucleotide resolution [19]. GTI-seq revealed a pronounced single peak highly focused at the annotated TIS with few reads recovered in the downstream region (Figure 1C, left panel). The lack of LTM-associated RPF reads at the 5th codon position strongly indicates that the ribosomal pausing at this position is a true elongation event. GTI-seq also permits identification of alternative start codons, including upstream TIS and downstream TIS sites [19]. To examine whether alternative initiation is also followed by downstream ribosomal pausing, we aligned transcripts by the alternative TIS sites identified by GTI-seq (Figure 1C, middle and right panels). Remarkably, the CHX-associated RPFs exhibit dominant peaks not only at the corresponding TIS positions, but also at the downstream 5th codon position. Thus, post-initiation pausing represents a universal feature for ribosomes after initiation from both the annotated and the alternative start codons.

When the ribosomal P-site is mapped at the 5th codon position, its footprint coincidently starts with AUG at the 5′ end. One possibility is that these RPFs are preferentially obtained after RNase I digestion or selectively amplified during deep sequencing. However, this is not the case. The frequency of RPFs with AUG at the 5′ end is among the average compared to RPFs starting with other sequences (Supplementary information, Figure S4). Furthermore, many internal AUG codons are not associated with the downstream pausing. Therefore, the elevated ribosome density at the 5th codon position after the annotated start codon is likely coupled with the initiation event.

Characterization of post-initiation pausing

To investigate possible mechanisms underlying post-initiation pausing at the 5th codon position, we first examined whether ribosome stalling at this specific position is sequence dependent. However, we found a similar codon composition at the 5th codon position to the one averaged across the entire CDS (Supplementary information, Figure S5). To find possible general relationships between the functions of genes and post-initiation pausing, we searched for common biological themes in transcripts with high and low ribosomal pausing at the 5th codon position. Gene ontology term analysis revealed no specific gene functions associated with either strong or weak post-initiation pausing (Supplementary information, Figure S6). These results indicate that the ribosomal pausing shortly after initiation is sequence independent, likely representing a translational event inherently associated with the translation machinery *per se*.

We next asked whether ribosomal pausing at the 5th codon position is a result of ribosomal stacking during elongation. To this end, we isolated the monosome fraction followed by Ribo-seq (Supplementary information, Figure S7). Since every transcript in the monosome has only one ribosome, the ribosome behavior is not influenced by any neighboring ribosomes. Despite much less RPF density in the CDS region, the monosome fraction maintained prominent peaks at both the start codon and the 5th codon position (Supplementary information, Figure S7). This result further supports the notion that post-initiation pausing reflects an intrinsic feature of ribosomes shortly after initiation.

Having characterized the post-initiation pausing in mammalian cells, we attempted to expand our findings to other species whose Ribo-seq data are available in the literature. Reanalyzing the RPF reads using the same pipeline revealed similar post-initiation pausing in other eukaryotic cells (Supplementary information, Figure S8), including budding yeast *S. cerevisiae* [11], nematode *C. elegans* [17], and zebrafish *D. rerio* [16]. Interestingly, the most recent report of mitochondrial ribosome profiling also showed similar ribosomal pausing at the 5th codon position [23]. Notably, the relative extent of post-initiation pausing varies among different studies and we cannot exclude the possibility that technical differences (e.g., Mg^{2+} concentration in polysome buffer) may cause variations of ribosome density at the 5th codon position. Considering its omnipresence in multiple species, it is likely that the post-initiation pausing is a general feature for different types of translation machinery.

Post-initiation pausing is attributed to the geometry of the exit tunnel

Given the sequence-independent but position-specific feature, the observed post-initiation pausing is likely governed by the ribosome exit tunnel. The interior of the ribosome exit tunnel is neither straight nor smooth with an evident constriction site formed by RPL4 and RPL17 [24] (Figure 2A). To investigate whether the highly focused ribosomal pausing shortly after initiation is attributed to the geometry of the exit tunnel, we focused on RPL4 because it is the first ribosomal protein that the nascent chain potentially interacts within the exit tunnel. We constructed a RPL4 mutant by deleting the most conserved HRSG loop region [25] (Supplementary information, Figure S9). After overexpression in HEK293 cells, myc-tagged RPL4(Δloop) mutant showed a similar cellular localization to the wild type (Figure 2B). In addition to the nucleolus localization that is typical for ribosome subunit assembly, both the wild-type and the mutant RPL4 showed the same cytoplasmic distribution as ribosomal P0, a protein associated only with the assembled ribosome complex. To confirm that RPL4(Δloop) is able to incorporate into the assembled 80S ribosome complex in the cytoplasm, we performed immunoprecipitation (IP) assay using an anti-myc antibody in HEK293 cells stably expressing wild-type RPL4 or RPL4(Δloop). The presence of a myc tag at the C terminus of the transgene prevents precipitation of ribosomes synthesizing the RPL4 polypeptide itself. In addition, we converted the polysome into monosome by RNase I digestion prior to anti-myc IP to exclude indirect ribosome pull-down (Figure 2C). Both small and large ribosomal proteins were readily precipitated by anti-myc antibody from cells expressing either wild-type RPL4 or RPL4(Δloop) (Figure 2C, lanes 5 and 6), but not GFP control. Thus, deleting

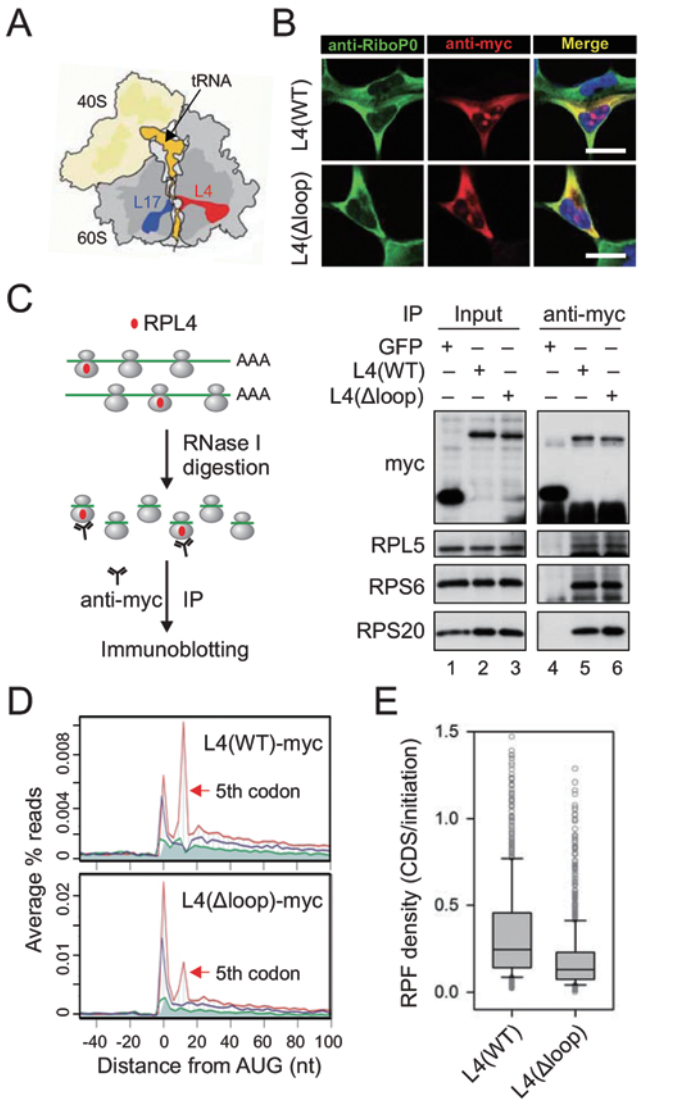

Figure 2 Reduced post-initiation pausing for ribosomes bearing L4 mutant. **(A)** Schematic structure of ribosomes highlighting the exit tunnel. tRNA and the nascent chain are shown in orange, RPL4 in red, and RPL17 in blue. **(B)** Cellular localization of L4 wild type and Δloop mutant is examined in HEK293 cells using immunostaining. Scale bar, 10 μm. **(C)** Myc-tagged L4 is incorporated into ribosome complexes. Polysome fractions from transfected HEK293 cells were treated with RNase I prior to anti-myc IP. Both the input and the immunoprecipitates were blotted using antibodies as indicated. **(D)** Metagene analysis of RPFs obtained from purified ribosomes bearing L4 wild type (top) and Δloop mutant (bottom). All mapped reads are aligned at the annotated start codon AUG and stratified by frames. **(E)** Read density over CDS relative to the initiation site (1st - 5th) is shown in box plots.

the loop region does not prevent RPL4 from integrating into the assembled 80S ribosome complexes.

We next examined the behavior of ribosomes bearing myc-tagged RPL4 by Ribo-seq of transfected cells. To exclude the RPFs derived from ribosomes containing endogenous RPL4, we conducted selective ribosome profiling by purifying myc-tagged ribosomes after RNase I digestion. Thus, all the obtained RPFs are exclusively derived from ribosomes bearing myc-tagged RPL4. As expected, ribosomes containing RPL4(WT) showed elevated ribosome density at both the start codon and the 5th codon positions (Figure 2D). However, RPL4(Δloop)-incorporated ribosomes exhibited a substantial reduction of ribosome density at the 5th codon position relative to the start codon (Figure 2D, bottom panel). The diminished post-initiation pausing is also evident on individual transcripts, including the relatively long *P4HB* and the short *RPL23* (Supplementary information, Figure S10). Notably, the ribosome density at the start codon remains high for ribosomes containing RPL4(Δloop), strongly indicating that the assembly of 80S ribosomes at the start codon is not affected by this ribosome variant.

Ribosomes with altered exit tunnel lead to abortive translation

For ribosomes with modified exit tunnel, the reduced post-initiation pausing is expected to promote the rate of translation. Yet the RPL4(Δloop)-associated RPFs showed an obvious decrease of footprint density over the downstream CDS region relative to the start codon (Figure 2E). This surprising finding suggests that the ribosome variant with a modified exit tunnel does not support continuous translation elongation. This could be explained by ribosome drop-off that occurs in the presence of RPL4(Δloop). To test this possibility, we inspected the distribution of myc-tagged RPL4 in ribosome fractions resolved by sucrose gradient velocity sedimentation (Figure 3A). Myc-tagged RPL4(WT) completely behaved like the endogenous one as evidenced by their nearly identical distribution in polysome fractions. RPL4(Δloop), in contrast, showed an evident decrease in the polysome fractions relative to the endogenous RPL4 despite its comparable enrichment in the monosome (Figure 3A and 3B). These results suggest that an altered ribosomal exit tunnel may cause ribosome dissociation shortly after initiation.

Notably, the distance between the peptidyltransferase center (PTC) and the RPL4 loop region is more than five amino acids [24]. Removing the RPL4 loop region does not seem to clog or close the exit tunnel as we observed no additional pausing sites within the 30-codon window for ribosomes bearing RPL4(Δloop) (Figure 2D). To examine whether translational abandonment mainly occurs before the nascent chain emerges out of the ribosome, we performed nascent chain IP in HEK293 cells expressing a GFP reporter with an N-terminal Flag-tag [8]. Early ribosome dissociation would prevent anti-Flag antibody from precipitating translating ribosomes. For cells expressing RPL4(WT), anti-Flag IP could pull down considerable amount of myc-tagged RPL4 along with other ribosome proteins (Figure 3C, lane 5). However, in cells expressing RPL4(Δloop), very little RPL4(Δloop) was co-precipitated by anti-Flag antibody when compared to other ribosome proteins (Figure 3C, lane 6). This result is consistent with early abandonment of translation for ribosomes with modified exit tunnel.

For ribosomes with altered exit tunnel, it is unclear which event happens first: reduced post-initiation pausing or ribosome dissociation. Although the lack of post-initiation pausing could trigger ribosome drop-off, it is equally possible that the diminished post-initiation pausing is a direct consequence of abolished translation shortly after initiation. In the latter scenario, dissociation of ribosomes bearing RPL4(Δloop) must occur before the nascent chain reaches the 5th codon position. Despite lots of efforts, we were unable to determine the length of tRNA-linked short peptides associated with ribosomes bearing RPL4(Δloop). Nevertheless, our results argue that the very first few amino acids are able to sense the integrity of the ribosomal exit tunnel in an active manner and post-initiation pausing of ribosomes may facilitate elongation commitment.

Ribosomes with altered exit tunnel lead to cellular toxicity

The frequent translational abandonment is expected to be detrimental to cellular functions. This was indeed the case. We examined cell viability after knocking down the endogenous RPL4 using lentiviruses expressing small hairpin RNA (shRNA) targeting the 3′ UTR of RPL4. Consistent with the essential role of RPL4 in protein production, we observed progressive cellular toxicity in control cells expressing GFP after RPL4 knockdown (Figure 4A). Only cells expressing wild-type RPL4, but not RPL4(loop), were able to maintain higher cell viability. Thus, the post-initiation pausing governed by the ribosomal exit tunnel represents an obligatory step between initiation and elongation.

Discussion

A longstanding question in translational control is to systemically understand physiological purposes of ribosomal pausing. mRNA structure, tRNA abundance, and amino acid sequence all have the potential to impact the

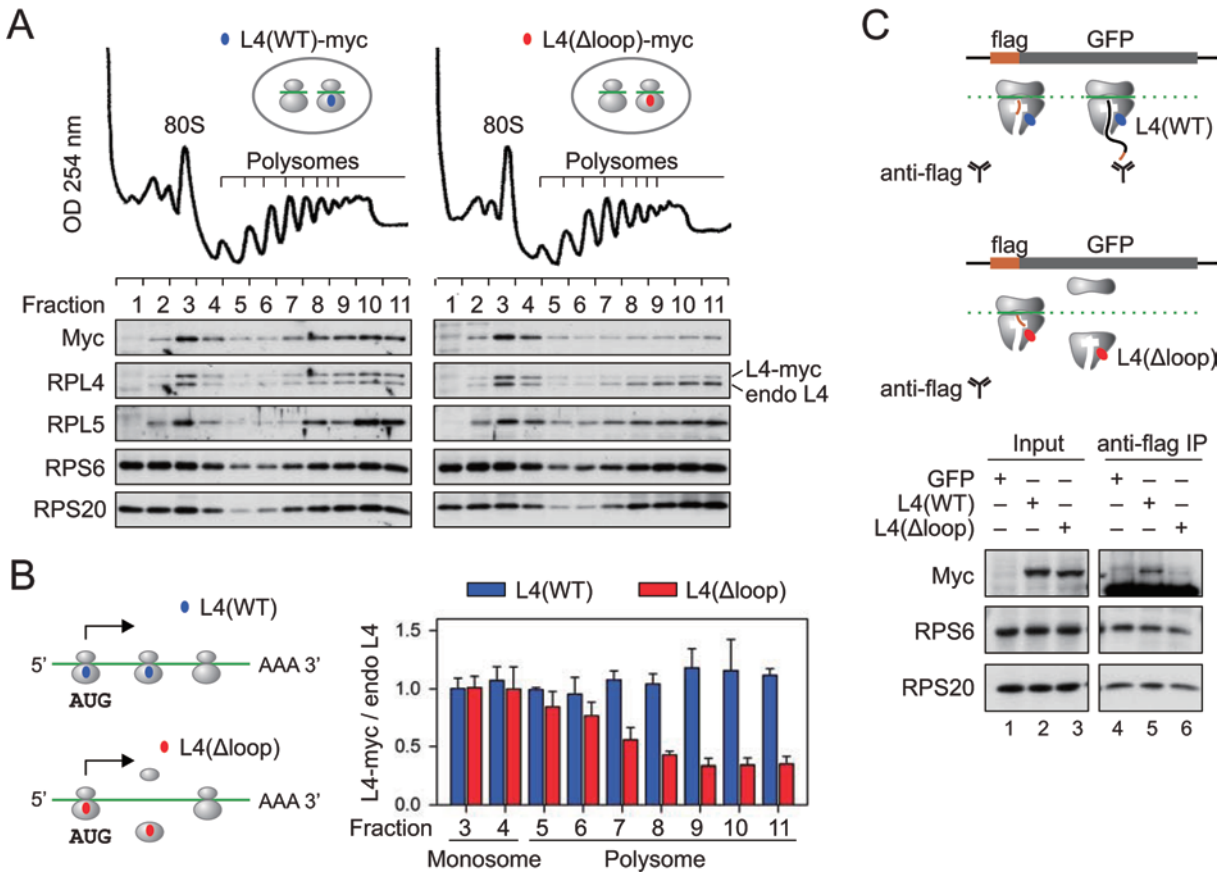

Figure 3 Ribosomes bearing L4 mutant lead to abortive translation. **(A)** Polysome profiles of HEK293 cells expressing L4 wild type or loop mutant. The bottom panel shows the distribution of exogenous and endogenous ribosome proteins in ribosome fractions. **(B)** A simple model of translational abandonment for ribosomes bearing L4(Δloop) mutant. The right panel shows the quantification of myc-tagged L4 relative to the endogenous L4 in ribosome fractions as shown in **A**. Data are shown as means ± SD, *n* = 3. **(C)** Schematic for nascent chain IP assay using a HEK293 cell line expressing flag-GFP (top panel). Transfected HEK293 cells were lysed and treated with RNase I prior to anti-flag IP. Both the input and the immunoprecipitates were blotted for ribosomal proteins as indicated (bottom panel).

ribosome dynamics. Based on multiple empirical data sets, here we report a sequence-independent but position-specific ribosomal pausing governed by the geometry of the exit tunnel. Several lines of evidence support the notion that the ribosome pausing at the 5th codon position serves as a functional signature of translation. First, post-initiation pausing of ribosomes is nearly a universal feature in a wide range of organisms. With an ever growing application of ribosome profiling in different cell types and tissues, we expect to see a more comprehensive picture illuminating ribosome dynamics between initiation and elongation. Second, we provide direct evidence that modifying the exit tunnel influences the extent of ribosomal pausing shortly after initiation. To our knowledge, this is the first example of ribosomal pausing associated with the translation machinery. Third, post-initiation pausing of ribosomes is of physiological significance as elimination of post-initiation pausing is coupled with translational abandonment. Together, these results argue that the ribosome behavior is intimately controlled via the constant interaction between the growing nascent chain and the translation machinery (Figure 4B).

It has long been believed that, after the assembly of 80S ribosome at the start codon, elongation ensues via a simple repetitive process comprising ribosomal translocation and tRNA recycling. However, a growing body of evidence suggests that the synthesis of the very first 4 amino acids possesses special features. In prokaryotes, the presence of macrolides allows synthesis of at least 4 amino acids before peptidyl-tRNA release even though the macrolide binding sites is far below the PTC [26]. It has also been reported that overexpression of very short

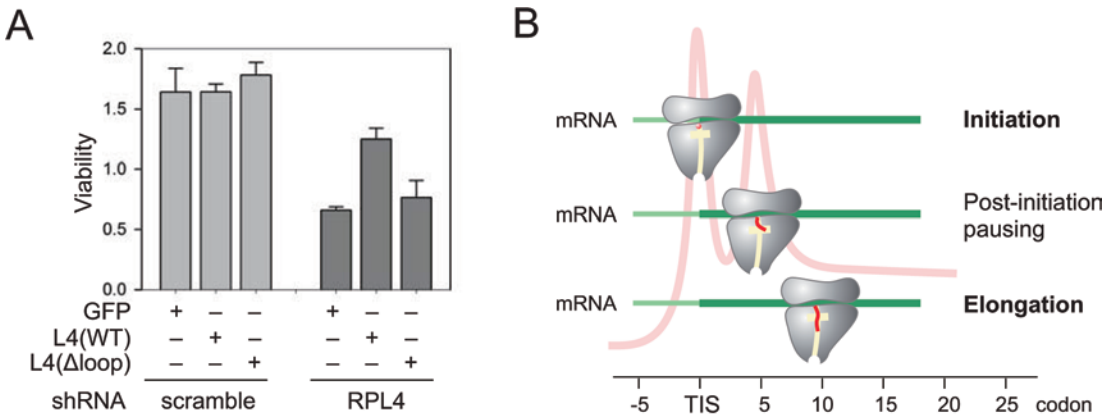

Figure 4 Physiological significance of post-initiation pausing. **(A)** HEK293 cells expressing GFP control, L4 wild type, or Δloop mutant were infected with lentiviruses encoding shRNA targeting endogenous L4 or scramble control. Cell viability was measured and quantified. Data are shown as means ± SD, *n* = 3. **(B)** A model for post-initiation pausing of ribosomes. After initiation, the nascent chain (red) traverses the exit tunnel (yellow). At the 5th codon position, the paused ribosome undergoes conformational changes, thereby facilitating elongation commitment by preventing nascent chain from off-route and abortive translation.

minigenes triggers ribosome drop-off. However, when the ORF length increased from three codons to seven, the drop-off frequency decreased significantly [27]. These findings can be explained by the existence of an additional step between initiation and elongation. It will be interesting to use single molecule fluorescence approach to elucidate ribosome dynamics in real time during the first several cycles of elongation [28].

The mandatory pausing of ribosomes at the 5th codon position is advantageous to ensure elongation commitment. The exit tunnel is the preferred but perhaps not the only pathway from the PTC. Some experimental results suggest that the nascent chain could leave the PTC along other routes [29]. We surmise that the post-initiation pausing of ribosomes allows the very first few amino acids to find the correct exit route. This unique interaction by the first amino acids could potentially trigger local conformational change of ribosomes before entering the exit tunnel. Interestingly, recent cryoelectron microscopy of eukaryotic ribosomes revealed discontinuous electron density of nascent chains after ~4 amino acids below the PTC [24], a strong indication of ribosome plasticity. In addition to RPL4, nascent chains undergo extensive interaction with many other ribosomal proteins, such as RPL17 and RPL39. Biochemical evidence suggested that the tunnel topology must be flexible to accommodate the nascent chain [30]. Given the unique feature of stalled ribosomes at the 5th codon position, post-initiation pausing of ribosomes represents a physiological signature of the translation machinery to ensure productive translation.

Materials and Methods

Cells and reagents

HEK293, HeLa, and MEF cells were maintained in Dulbecco's Modified Eagle's Medium (DMEM) with 10% fetal bovine serum (FBS). CHX, puromycin, and erythromycin were purchased from Sigma. LTM was provided by Ben Shen (Scripps Florida) as described previously [19]. Anti-RPS6 antibody was purchased from Cell Signaling Technology; anti-myc from Santa Cruz Biotechnology; a human polyclonal autoimmune antisera targeting ribosomal P is from Immunovision; anti-flag, anti-RPS20, and anti-RPL5 antibodies from Sigma. Plasmid transfection was performed using Lipofectamine 2000 (Invitrogen) following the manufacturer's instruction.

Plasmids and lentiviral shRNAs

The full-length *RPL4* gene was amplified by PCR followed by direct cloning into pcDNA3.1-myc-His vector (Invitrogen). To construct the *RPL4(Δloop)* mutant, RPL4 fragments corresponding to CDS 1-252 nt and 262-1 281 nt were amplified by PCR followed by ligation using a *Bam*HI restriction site. RPL4 shRNA targeting sequences (human: 5′-TGAATAAAGACCTGATTATAC-3′) and control sequence (5′-AACAGTCGCGTTTGCGACTGG-3′) were designed based on RNAi consortium at Broad Institute (http://www.broad mit.edu/rnai/trc). All shRNA targeting sequences were cloned into DECIPHER™ pRSI9-U6-(sh)-UbiC-TagRFP-2A-Puro (CELLECTA). Lentiviral particles were packaged using Lenti-X 293T cells (Clontech). Virus-containing supernatants were collected at 48 h after transfection and target cells were infected in the presence of 8 μg/ml polybrene.

Immunofluorescence staining

Cells grown on glass coverslips were fixed in 4% paraformaldehyde and permeabilized by 0.2% Triton X-100. After blocking

in 2% BSA in PBS, fixed cells were incubated with the primary antibody at 4 °C overnight followed by 1-h incubation at room temperature with Alexa Fluor-labeled secondary antibodies. Cells were then washed with PBS and incubated for 5 min in PBS supplemented with Hoechst to counter-stain the nuclei. After a final wash with PBS, coverslips were mounted onto slides and viewed using a confocal microscope (Zeiss LSM710).

Immunoprecipitation

Cells were harvested in ice-cold lysis buffer (10 mM Hepes, pH 7.4, 100 mM KCl, 5 mM $MgCl_2$, 100 μg/ml CHX) and lysed with Lysing Matrix D (Fisher). After centrifugation at 4 °C and 10 000× *g* for 10 min, supernatant was collected, and treated with RNase I (Ambion) at 4 °C for 1 h. Digestion was neutralized with SUPERase inhibitor (SUPERase_In, Ambion) and the samples were incubated with anti-myc beads (Sigma) or anti-flag beads (Sigma) at 4 °C overnight. Immunoprecipitates were washed 3 times with lysis buffer. The washed beads were resuspended in 1× SDS sample buffer (100 mM Tris, pH 6.8, 2% SDS, 15% glycerol, 5% β-mercaptoethanol, 0.1% bromophenol blue), boiled for 5 min, and analyzed by immunoblotting.

Immunoblotting

Proteins were resolved on SDS-PAGE and transferred to Immobilon-P membranes (Millipore). Membranes were blocked for 1 h in TBS containing 5% BSA, followed by incubation with primary antibodies. After incubation with horseradish peroxidase-coupled secondary antibodies, immunoblots were developed using enhanced chemiluminescence (ECLPlus, GE Healthcare).

Cell viability assay

HEK293 stable cell lines expressing GFP control, L4 wild type, or Δloop mutant were infected with lentiviruses encoding shRNA targeting RPL4 or scramble control. 48 h after infection, cells were trypsinized and plated at equal density to the 96-well plate. Cell viability was measured on day 3 using CCK-8 kit (Dojindo Molecular Technologies) according to the manufacturer's instructions.

Ribosome profiling

Sucrose solutions were prepared in polysome gradient buffer (10 mM Hepes, pH 7.4, 100 mM KCl, 5 mM $MgCl_2$, 100 μg/ml CHX, 5 mM DTT, and 20 U/ml SUPERase_In (Ambion)). Sucrose density gradients (15% - 45% (wt/vol)) were freshly made in SW41 ultracentrifuge tubes (Fisher) using a BioComp Gradient Master (BioComp) according to the manufacturer's instructions. Cells were plated to four 10-cm dishes before ribosome profiling. HEK293 cells were first treated with CHX (100 μM) or LTM (50 μM) for 30 min at 37 °C to freeze the translating ribosomes or initiating ribosomes, respectively. After ice-cold PBS solution wash, cells were then harvested by ice-cold polysome lysis buffer (10 mM Hepes, pH 7.4, 100 mM KCl, 5 mM $MgCl_2$, 100 μg/ml CHX, 5 mM DTT, 20 U/ml SUPERase_In, and 2% (vol/vol) Triton X-100). After centrifugation at 4 °C and 10 000× *g* for 10 min, approximately 650 μl supernatant was loaded onto sucrose gradients, followed by centrifugation for 100 min at 38 000 rpm, 4 °C, in an SW41 rotor. Separated samples were fractionated at 0.375 ml/min by using a fractionation system (Isco) that continually monitored OD254 values. Fractions were collected into tubes at 1-min intervals. To convert the polysome into monosome, *E. coli* RNase I (Ambion) was added into the pooled polysome samples (750 U per 100 A260 units) and incubated at 4 °C for 1 h. SUPERase_In (50 U per 100 U RNase I) was then added to stop digestion. Total RNA extraction was performed using TRIzol reagent.

cDNA library construction of RPF

Purified RNA samples were dephosphorylated in a 15 μl reaction containing 1× T4 polynucleotide kinase buffer, 10 U SUPERase_In, and 20 U T4 polynucleotide kinase (NEB). Dephosphorylation was carried out for 1 h at 37 °C, and the enzyme was then heat inactivated for 20 min at 65 °C. Dephosphorylated samples were then mixed with 2 Novex TBE-Urea sample buffer (Invitrogen) and loaded on a Novex denaturing 15% polyacrylamide TBE-urea gel (Invitrogen). The gel was stained with SYBR Gold (Invitrogen) to visualize the RNA fragments. Gel bands containing RNA species corresponding to 28 nt were excised and physically disrupted by centrifugation through the holes of the tube. RNA fragments were dissolved by soaking overnight in gel elution buffer (300 mM NaOAc, pH 5.5, 1 mM EDTA, 0.1 U/ml SUPERase_In). The gel debris was removed using a Spin-X column (Corning) and RNA was purified by using ethanol precipitation. Purified RNA fragments were resuspended in 10 mM Tris (pH 8) and denatured briefly at 65 °C for 30 s. Poly-(A) tailing reaction was performed in a 8 μl buffer with 1× poly-(A) polymerase, 1 mM ATP, 0.75 U/μl SUPERase_In, and 3 U *E. coli* poly-(A) polymerase (NEB). Tailing was carried out for 45 min at 37 °C. For reverse transcription, the following oligos containing barcodes were synthesized:

MCA02, 5′-pCAGATCGTCGGACTGTAGAACTCT/idSp/CAAGCAGAAGACGGCATACGATTTTTTTTTTTTTTTTTTTVN-3′;
LGT03, 5′-pGTGATCGTCGGACTGTAGAACTCT/idSp/CAAGCAGAAGACGGCATACGATTTTTTTTTTTTTTTTTTTVN-3′;
YAG04, 5′-pTCGATCGTCGGACTGTAGAACTCT/idSp/CAAGCAGAAGACGGCATACGATTTTTTTTTTTTTTTTTTTVN-3′;
HTC05, 5′-pAGGATCGTCGGACTGTAGAACTCT/idSp/CAAGCAGAAGACGGCATACGATTTTTTTTTTTTTTTTTTTVN-3′.

In brief, the tailed RNA product was mixed with 0.5 mM dNTP and 2.5 mM synthesized primer and incubated at 65 °C for 5 min, followed by incubation on ice for 5 min. The reaction mix was then added with 20 mM Tris (pH 8.4), 50 mM KCl, 5 mM $MgCl_2$, 10 mM DTT, 40 U RNaseOUT, and 200 U SuperScript III (Invitrogen). Reverse transcription reaction was performed according to the manufacturer's instructions. RNA was eliminated from cDNA by adding 1.8 μl of 1 M NaOH and incubating at 98 °C for 20 min. The reaction was then neutralized with 1.8 μl of 1 M HCl. Reverse transcription products were separated on a 10% polyacrylamide TBE-urea gel as described earlier. The extended first-strand product band was expected to be approximately 100 nt, and the corresponding region was excised. The cDNA was recovered by using DNA gel elution buffer (300 mM NaCl, 1 mM EDTA). First-strand cDNA was circularized in 20 μl of reaction containing 1× CircLigase buffer, 2.5 mM MnCl2, 1M Betaine, and 100 U CircLigase II (Epicentre). Circularization was performed at 60 °C for 1 h, and the reaction was heat inactivated at 80 °C for 10 min. Circular single-strand DNA was relinearized with 20 mM Tris-acetate, 50 mM potassium acetate, 10 mM magnesium acetate, 1 mM DTT, and 7.5 U APE 1 (NEB). The reaction was carried out at 37 °C for 1 h. The linearized single-strand DNA was separated on a Novex 10% polyacrylamide TBE-urea gel (Invitrogen) as described earlier. The expected 100-nt product bands were excised and recovered as

described earlier.

Deep sequencing

Single-stranded template was amplified by PCR using the Phusion High-Fidelity enzyme (NEB) according to the manufacturer's instructions. The oligonucleotide primers qNTI200 (5′-CAAGCAGAAGACGGCATA-3′) and qNTI201 (5′-AATGATACGGCGACCACCGACAGGTTCAGAGTTCTACAGTCCGACG-3′) were used to create DNA suitable for sequencing, i.e., DNA with Illumina cluster generation sequences on each end and a sequencing primer binding site. The PCR contains 1× HF buffer, 0.2 mM dNTP, 0.5 μM oligonucleotide primers, and 0.5 U Phusion polymerase. PCR was carried out with an initial 30-s denaturation at 98 °C, followed by 12 cycles of 10-s denaturation at 98 °C, 20-s annealing at 60 °C, and 10 s extension at 72 °C. PCR products were separated on a nondenaturing 8% polyacrylamide TBE gel as described earlier. Expected DNA at 120 bp was excised and recovered as described earlier. After quantification by Agilent BioAnalyzer DNA 1000 assay, equal amount of barcoded samples were pooled into one sample. Approximately 3-5 pM mixed DNA samples were used for cluster generation followed by sequencing using sequencing primer 5′-CGACAGGTTCAGAGTTCTACAGTCCGACGATC-3′ (Illumina Genome Analyzer 2 or HiSeq).

Data analysis

Barcoded reads were separated into individual data file for each sample according to the 5′ end 2-nt barcode sequences. Seven nucleotides were trimmed from the 3′ end of each 50-nt-long Illumina sequence read to remove adaptor sequences, and the poly (A) tails were removed from the 3′ end, allowing one mismatch. Reads between 25 and 35 nt in length were mapped using Bowtie [31] to the sense strand of the longest Refseq transcripts for each human gene. One mismatch was allowed in all mappings; in cases of multiple mapping, mismatched positions were not used if a perfect match existed. Reads mapped more than 100 times were discarded to remove poly-A-derived reads. Finally, reads were counted at every position of individual transcripts by using the 13th nucleotide of the read for the P-site position.

To generate aggregation plots, the number of RPF reads aligned to each position of individual transcripts was first normalized by the read density within 50-150 codon window, which was considered as the representative translational level of the transcript. Only transcripts with CDS longer than 150 codons and with minimum read density of 25 rpkM were used for aggregation plots. The read counts were then averaged across all transcripts for each position relative to the annotated start codon based on Refseq.

The framing of reads mapped to the 1st codon, 5th codon, or entire CDS was calculated relative to the annotated ORF based on Refseq. The length distribution was also calculated for reads mapped to the 1st codon, the 5th codon, or the entire CDS. Read density over the CDS (6-stop codon) relative to the initiation site (1-5 codon) was computed for each transcript. Only transcripts with minimum read density of 10 rpkM over the CDS and minimum 5 reads at the initiation site were used to calculate the ratios.

For codon composition analysis, the annotated CDS from human gene was downloaded from UCSC table browser. The codon composition of the 1st codon, 5th codon, and whole CDS were summarized based on the longest transcripts of human genes.

For GO term enrichment analysis, two groups of genes were collected based on the average read densities in the regions flanking the start codon and the 5th codon by the following criteria:

Group I: $Density_{1st\ codon} > 1.2 \times Density_{5th\ codon}$

Group II: $Density_{5th\ codon} > 1.2 \times Density_{5th\ codon}$

The gene ontology analyses were conducted on the above two groups of genes using DAVID [32].

Acknowledgments

We thank members of the Qian laboratory for critical reading of the manuscript and Dr Jonathan Yewdell (NIAID, NIH) for providing anti-puromycin monoclonal antibody. B L is partly supported by the Genomics Scholar's Award from Center for Vertebrate Genomics at Cornell. This work was supported by grants from National Institutes of Health (1 DP2 OD006449-01), Ellison Medical Foundation (AG-NS-0605-09), and DOD Exploration-Hypothesis Development Award (W81XWH-11-1-0236) to S-B Q.

References

1 Buchan JR, Stansfield I. Halting a cellular production line: responses to ribosomal pausing during translation. *Biol Cell* 2007; **99**:475-487.

2 Kertesz M, Wan Y, Mazor E, *et al.* Genome-wide measurement of RNA secondary structure in yeast. *Nature* 2010; **467**:103-107.

3 Plotkin JB, Kudla G. Synonymous but not the same: the causes and consequences of codon bias. *Nat Rev Genet* 2011; **12**:32-42.

4 Kramer G, Boehringer D, Ban N, Bukau B. The ribosome as a platform for co-translational processing, folding and targeting of newly synthesized proteins. *Nat Struct Mol Biol* 2009; **16**:589-597.

5 Farabaugh PJ. Translational frameshifting: implications for the mechanism of translational frame maintenance. *Prog Nucleic Acid Res Mol Biol* 2000; **64**:131-170.

6 Doma MK, Parker R. Endonucleolytic cleavage of eukaryotic mRNAs with stalls in translation elongation. *Nature* 2006; **440**:561-564.

7 Komar AA. A pause for thought along the co-translational folding pathway. *Trends Biochem Sci* 2009; **34**:16-24.

8 Liu B, Han Y, Qian SB. Cotranslational response to proteotoxic stress by elongation pausing of ribosomes. *Mol Cell* 2013; **49**:453-463.

9 Shalgi R, Hurt JA, Krykbaeva I, Taipale M, Lindquist S, Burge CB. Widespread regulation of translation by elongation pausing in heat shock. *Mol Cell* 2013; **49**:439-452.

10 Wolin SL, Walter P. Ribosome pausing and stacking during translation of a eukaryotic mRNA. *EMBO J* 1988; **7**:3559-3569.

11 Ingolia NT, Ghaemmaghami S, Newman JR, Weissman JS. Genome-wide analysis *in vivo* of translation with nucleotide resolution using ribosome profiling. *Science* 2009; **324**:218-223.

12 Guo H, Ingolia NT, Weissman JS, Bartel DP. Mammalian microRNAs predominantly act to decrease target mRNA levels. *Nature* 2010; **466**:835-840.

13 Brar GA, Yassour M, Friedman N, Regev A, Ingolia NT, Weissman JS. High-resolution view of the yeast meiotic pro-

gram revealed by ribosome profiling. *Science* 2012; **335**:552-557.
14 Oh E, Becker AH, Sandikci A, *et al.* Selective ribosome profiling reveals the cotranslational chaperone action of trigger factor *in vivo*. *Cell* 2011; **147**:1295-1308.
15 Li GW, Oh E, Weissman JS. The anti-Shine-Dalgarno sequence drives translational pausing and codon choice in bacteria. *Nature* 2012; **484**:538-541.
16 Bazzini AA, Lee MT, Giraldez AJ. Ribosome profiling shows that miR-430 reduces translation before causing mRNA decay in zebrafish. *Science* 2012; **336**:233-237.
17 Stadler M, Artiles K, Pak J, Fire A. Contributions of mRNA abundance, ribosome loading, and post- or peri-translational effects to temporal repression of *C. elegans* heterochronic miRNA targets. *Genome Res* 2012; **22**:2418-2426.
18 Gerashchenko MV, Lobanov AV, Gladyshev VN. Genome-wide ribosome profiling reveals complex translational regulation in response to oxidative stress. *Proc Natl Acad Sci USA* 2012; **109**:17394-17399.
19 Lee S, Liu B, Huang SX, Shen B, Qian SB. Global mapping of translation initiation sites in mammalian cells at single-nucleotide resolution. *Proc Natl Acad Sci USA* 2012; **109**:E2424-E2432.
20 Guydosh NR, Green R. Dom34 rescues ribosomes in 3′ untranslated regions. *Cell* 2014; **156**:950-962.
21 O'Connor PB, Li GW, Weissman JS, Atkins JF, Baranov PV. rRNA:mRNA pairing alters the length and the symmetry of mRNA-protected fragments in ribosome profiling experiments. *Bioinformatics* 2013; **29**:1488-1491.
22 Schneider-Poetsch T, Ju J, Eyler DE, *et al.* Inhibition of eukaryotic translation elongation by cycloheximide and lactimidomycin. *Nat Chem Biol* 2010; **6**:209-217.
23 Rooijers K, Loayza-Puch F, Nijtmans LG, Agami R. Ribosome profiling reveals features of normal and disease-associated mitochondrial translation. *Nat Commun* 2013; **4**:2886.
24 Wilson DN, Beckmann R. The ribosomal tunnel as a functional environment for nascent polypeptide folding and translational stalling. *Curr Opin Struct Biol* 2011; **21**:274-282.
25 Klinge S, Voigts-Hoffmann F, Leibundgut M, Arpagaus S, Ban N. Crystal structure of the eukaryotic 60S ribosomal subunit in complex with initiation factor 6. *Science* 2011; **334**:941-948.
26 Starosta AL, Karpenko VV, Shishkina AV, *et al.* Interplay between the ribosomal tunnel, nascent chain, and macrolides influences drug inhibition. *Chem Biol* 2010; **17**:504-514.
27 Heurgue-Hamard V, Mora L, Guarneros G, Buckingham RH. The growth defect in Escherichia coli deficient in peptidyl-tRNA hydrolase is due to starvation for Lys-tRNA(Lys). *EMBO J* 1996; **15**:2826-2833.
28 Petrov A, Kornberg G, O'Leary S, Tsai A, Uemura S, Puglisi JD. Dynamics of the translational machinery. *Curr Opin Struct Biol* 2011; **21**:137-145.
29 Tenson T, Ehrenberg M. Regulatory nascent peptides in the ribosomal tunnel. *Cell* 2002; **108**:591-594.
30 Zhang Y, Wolfle T, Rospert S. Interaction of nascent chains with the ribosomal tunnel proteins Rpl4, Rpl17, and Rpl39 of Saccharomyces cerevisiae. *J Biol Chem* 2013; **288**:33697-33707.
31 Langmead B, Trapnell C, Pop M, Salzberg SL. Ultrafast and memory-efficient alignment of short DNA sequences to the human genome. *Genome Biol* 2009; **10**:R25.
32 Huang da W, Sherman BT, Lempicki RA. Systematic and integrative analysis of large gene lists using DAVID bioinformatics resources. *Nat Protoc* 2009; **4**:44-57.

(**Supplementary information** is linked to the online version of the paper on the *Cell Research* website.)

Quantitative profiling of initiating ribosomes *in vivo*

Xiangwei Gao[1,5,6], Ji Wan[1,6], Botao Liu[2], Ming Ma[3], Ben Shen[3,4] & Shu-Bing Qian[1,2]

Cells have evolved exquisite mechanisms to fine-tune the rate of protein synthesis in response to stress. Systemic mapping of start-codon positions and precise measurement of the corresponding initiation rate would transform our understanding of translational control. Here we present quantitative translation initiation sequencing (QTI-seq), with which the initiating ribosomes can be profiled in real time at single-nucleotide resolution. Resultant initiation maps not only delineated variations of start-codon selection but also highlighted a dynamic range of initiation rates in response to nutrient starvation. The integrated data set provided unique insights into principles of alternative translation and mechanisms controlling different aspects of translation initiation. With RiboTag mice, QTI-seq permitted tissue-specific profiling of initiating ribosomes *in vivo*. Liver cell–specific ribosome profiling uncovered a robust translational reprogramming of the proteasome system in fasted mice. Our findings illuminated the prevalence and dynamic nature of translational regulation pivotal to physiological adaptation *in vivo*.

Translational regulation permits cells to respond swiftly to stress conditions via immediate and selective changes in protein expression levels[1–3]. Much of this translational control occurs at the initiation stage[4–7]. Although the importance of translation initiation has long been appreciated, direct measurement of the initiation rate on individual mRNAs has been difficult. Recent development of ribosome-profiling technology (Ribo-seq), based on deep sequencing of ribosome-protected mRNA fragments (RPFs), enables monitoring of ribosome dynamics with unprecedented resolution at the genome-wide scale[8,9]. The obtained snapshot of ribosome occupancy on the coding region has often been used to estimate relative changes of translation efficiency under different growth conditions. A caveat, however, exists because the average ribosome density on mRNAs is negatively influenced by the elongation speed[10,11]. Dynamic changes of initiation rates are thus masked by the varied elongation speed under different growth conditions. In addition, the average density of ribosome occupancy is not suitable to evaluate alternative translation events occurring on the same mRNA[12]. These constraints point to a need for a method capable of mapping start-codon selection and quantifying the rate of 80S ribosome assembly at individual translation initiation sites (TISs).

Much of our understanding of the basic mechanisms of translation initiation is limited to cells in culture. Investigating translational control at the organismal level remains a pressing and formidable challenge. The cellular heterogeneity of tissues and organs confounds our efforts to achieve cell type–specific genomic and proteomic interrogation. To monitor protein synthesis at the organismal level, one approach relies on tagged ribosomal proteins, such as hemagglutinin (HA)-tagged Rpl22 (ref. 13) or EGFP-fused Rpl10a (ref. 14). Following genetic targeting to specific cell populations, affinity purification allows isolation of polysome-bound mRNAs from specific cell types suitable for profiling assays. However, current methods do not allow tissue-specific profiling of initiating ribosomes, which bear more reliable information in evaluating translational control *in vivo*.

Here we present an approach called QTI-seq that allows comprehensive monitoring of translation initiation in cells and solid tissues. Together with the RNA-seq and Ribo-seq data sets acquired in parallel, the integrated ribosome-profiling data afford a holistic view of the translational landscape under different growth conditions.

RESULTS

QTI-seq captures initiating ribosomes in an unbiased manner

We previously developed global translation initiation sequencing (GTI-seq)[15], which capitalizes on the unique feature of lactimidomycin (LTM) that preferentially acts on the first 80S ribosome when its E site is empty[16]. However, LTM-mediated enrichment of initiating ribosomes requires an incubation of the cell at 37 °C to allow for the release of elongating ribosomes. This procedure, albeit essential for high-resolution mapping of TISs, may generate a number of artifacts. First, free ribosomes could start new rounds of initiation during the incubation period, resulting in an amplification of ribosome occupancy at the start codon (**Supplementary Fig. 1a**). Second, the amplified ribosome density is biased toward the upstream initiators, causing an unwanted 5′-end inflation of RPFs. When GTI-seq was applied to human HEK293 cells with amino acid deprivation, the LTM peaks at the annotated start codons (aTISs) showed few changes despite the pervasive reduction of ribosome occupancy on many transcripts

[1]Division of Nutritional Sciences, Cornell University, Ithaca, New York, USA. [2]Graduate Field of Genetics, Genomics & Development, Cornell University, Ithaca, New York, USA. [3]Department of Chemistry, The Scripps Research Inst tute, Jupiter, Florida, USA. [4]Molecular Therapeutics and Natural Products Library Initiative, The Scripps Research Institute, Jupiter, Florida, USA. [5]Present address: Institute of Environmental Medicine, Zhejiang University School of Medicine, Hangzhou, People's Republic of China. [6]These authors contributed equally to this work. Correspondence should be addressed to S.-B.Q. (sq38@cornell.edu).

RECEIVED 1 AUGUST; ACCEPTED 30 OCTOBER; PUBLISHED ONLINE 8 DECEMBER 2014; DOI:10.1038/NMETH.3208

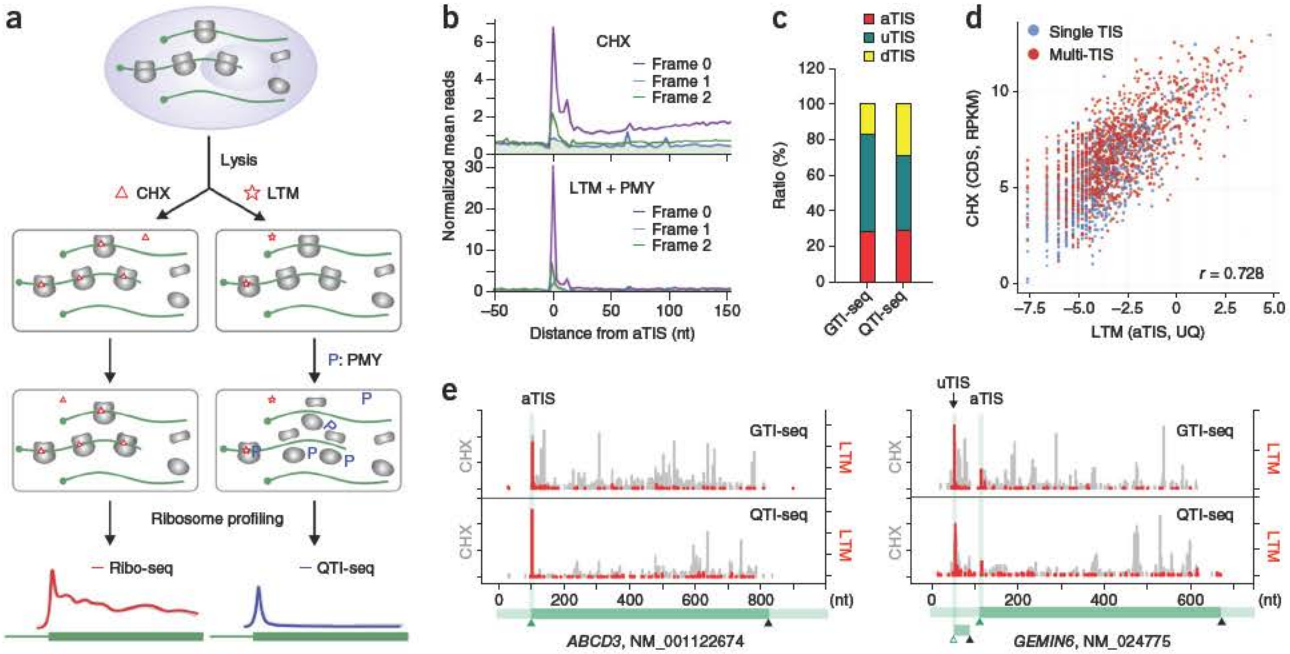

Figure 1 | QTI-seq captures real-time translation initiation events in a qualitative and quantitative manner. (**a**) Schematic of Ribo-seq (left) and QTI-seq (right) procedures. CHX, cycloheximide; LTM, lactimidomycin; PMY, puromycin. (**b**) Meta-gene analysis of CHX-associated ribosome density and LTM-associated ribosome density in HEK293 cells captured by QTI-seq. Normalized ribosome-protected mRNA fragment (RPF) reads are averaged across the entire transcriptome and aligned at the annotated start codon (aTIS). Different reading frames are separated and color coded. (**c**) Relative ratios of different types of TISs identified by GTI-seq or QTI-seq in HEK293 cells. uTIS, upstream TIS; dTIS, downstream TIS. (**d**) Correlation between LTM-associated aTIS density, normalized by upper quartile (UQ), and CHX-associated coding region (CDS) ribosome occupancy, normalized by reads per kilobase per million reads (RPKM). Genes with a single aTIS or multiple TISs are shown as blue and red dots, respectively. (**e**) Examples of single-TIS (*ABCD3*) and multiple-TIS (*GEMIN6*) genes revealed by GTI-seq (top) and QTI-seq (bottom). The *y*-axis scales are identical. The corresponding gene structure is shown below the *x* axis.

(**Supplementary Fig. 1b**). As a result, virtually no correlation was found between the differences of LTM-captured aTIS density and the ribosome occupancy on the coding region (CDS) (**Supplementary Fig. 1c**). The lack of quantitative features in GTI-seq largely hampers comparative interrogation of translational regulation.

To circumvent this limitation, we set out to devise QTI-seq to preserve the small population of initiating ribosomes with minimal perturbation. Following extensive optimization, we implemented three steps to achieve this goal: (i) rapidly break down cells using lysing matrix D, which has a minimal effect on ribosome stability; (ii) specifically freeze the initiating ribosomes by treating cell lysates with LTM; and (iii) effectively deplete the elongating ribosomes by introducing another translation inhibitor, puromycin (PMY) (**Fig. 1a**). PMY does not affect translation initiation and has been used previously to enrich the initiating ribosomes[17]. Acting as a tRNA analog, PMY releases the nascent chain and dissociates the ribosome into separate subunits[18]. In the presence of elongation inhibitors such as cycloheximide (CHX), however, addition of PMY catalyzes puromycylation of the nascent chain without triggering ribosome dissociation[19]. The same feature holds true for cell-free samples as the presence of CHX completely prevented PMY-induced polysome disassembly (**Supplementary Fig. 2**). Because LTM uses a similar mechanism to that of CHX but selectively acts on the first 80S ribosome[16], we reasoned that sequential treatment with LTM and PMY would dissociate the elongating ribosomes but leave the initiating ribosomes insensitive to PMY (**Fig. 1a**). Indeed, PMY addition in the presence of LTM resulted in polysome disassembly with a corresponding increase of the monosome (**Supplementary Fig. 2**). To examine whether the increased monosome contained the preserved initiating ribosomes, we purified RPFs followed by deep sequencing. Metagene analysis revealed that the LTM-associated RPF reads were highly enriched at the aTIS codon (**Fig. 1b**). Additionally, the aTIS ribosome density captured by LTM was highly reproducible (**Supplementary Fig. 3**).

Because QTI-seq captured a small population of initiating ribosomes without 5′-end RPF inflation, QTI-seq identified fewer total TISs than GTI-seq in HEK293 cells (5,099 vs. 13,915), especially the upstream TIS codons (uTISs) (**Fig. 1c**). Consistent with previous reports[15,20], codon composition analysis revealed that more than half the TISs used a non-AUG sequence as the translation initiator (**Supplementary Fig. 4**). The associated LTM peak height at the aTISs showed a strong correlation with the average ribosome occupancy along the corresponding CDS ($r = 0.728$; **Fig. 1d**). In addition to this quantitative feature, QTI-seq retained the high precision in mapping TIS positions at a single-nucleotide resolution. For instance, a prominent LTM peak was located exactly at the annotated start codon of *ABCD3*; an out-of-frame uTIS was uncovered in *GEMIN6* (**Fig. 1e**). QTI-seq thus offers a promising approach to exploring real-time translation initiation in a qualitative and quantitative manner.

Quantitative TIS profile in response to starvation

We next applied QTI-seq to HEK293 cells with amino acid deprivation (**Supplementary Fig. 5**). Total cellular RNA was also

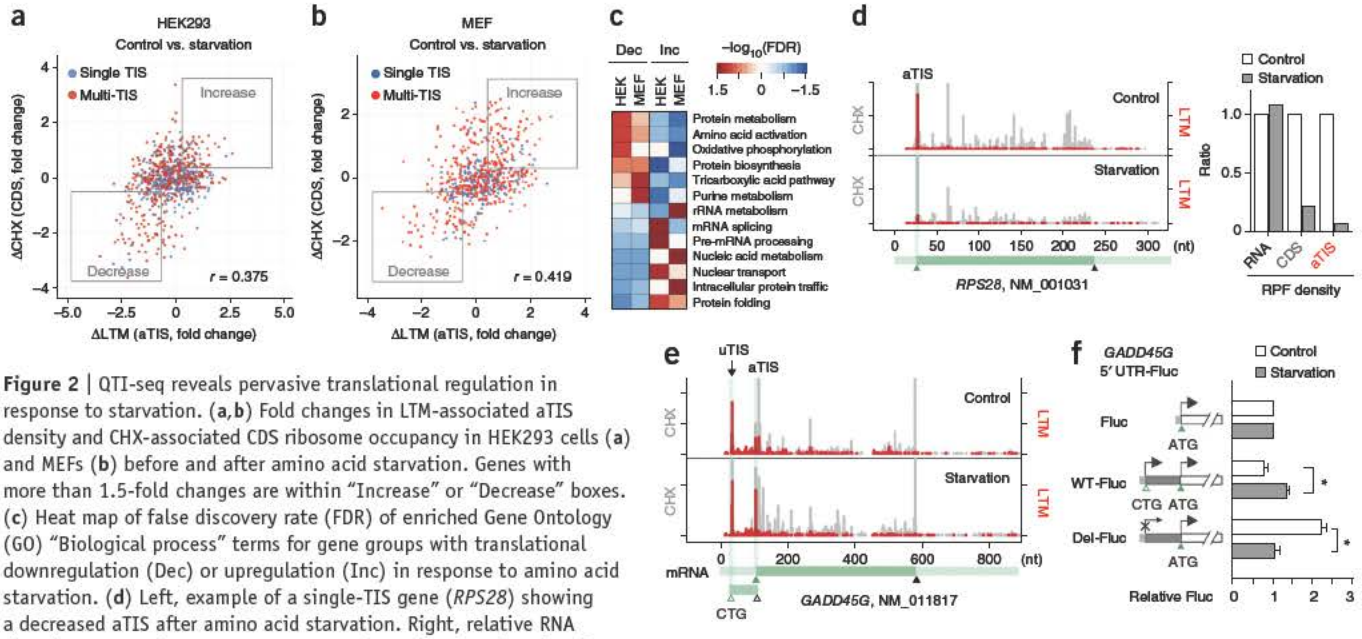

Figure 2 | QTI-seq reveals pervasive translational regulation in response to starvation. (**a**,**b**) Fold changes in LTM-associated aTIS density and CHX-associated CDS ribosome occupancy in HEK293 cells (**a**) and MEFs (**b**) before and after amino acid starvation. Genes with more than 1.5-fold changes are within "Increase" or "Decrease" boxes. (**c**) Heat map of false discovery rate (FDR) of enriched Gene Ontology (GO) "Biological process" terms for gene groups with translational downregulation (Dec) or upregulation (Inc) in response to amino acid starvation. (**d**) Left, example of a single-TIS gene (*RPS28*) showing a decreased aTIS after amino acid starvation. Right, relative RNA abundance, CDS ribosome occupancy and aTIS ribosome density of *RPS28*. (**e**) Example of a multiple-TIS gene (*GADD45G*) showing an increased aTIS fraction after amino acid starvation. (**f**) Experimental validation of translational control of GADD45G by a firefly luciferase (Fluc) reporter bearing the 5′ UTR of *GADD45G* with (WT) or without the uTIS codon CTG (Del). Data are mean ± s.e.m.; $n = 3$ biological replicates; $^*P < 0.05$ by Student's *t*-test.

collected in parallel for RNA-seq to quantify mRNA abundance. In response to starvation, the changes in the initiation rates showed positive correlation with the differences of ribosome occupancy on the corresponding CDS ($r = 0.375$; **Fig. 2a**). The same observation held for a mouse embryonic fibroblast (MEF) cell line subjected to starvation ($r = 0.419$; **Fig. 2b**). The imperfect correlation was partially due to reduced elongation speed under nutrient starvation that potentially increases the CDS ribosome occupancy (**Supplementary Fig. 6**). From the comprehensive data sets acquired from QTI-seq and Ribo-seq, we identified a large number of transcripts that underwent twofold changes upon starvation (1,073 in HEK293 cells and 820 in MEFs; **Supplementary Tables 1** and **2**). Among the genes showing repressed translation, many of them are involved in protein biosynthesis and metabolism (**Fig. 2c**). As a typical example, the gene encoding ribosomal protein RPS28 showed a nearly fivefold decrease in ribosome occupancy on the CDS in response to starvation (**Fig. 2d**). Remarkably, QTI-seq displayed a decrease greater than 14-fold in the ribosome density at the start codon of *RPS28*. Without the negative influence imposed by elongation speed variation, QTI-seq sets itself apart from previous methods by reporting true measures of initiation rates.

QTI-seq also captured a considerable number of genes whose transcripts experienced increased initiation in response to starvation (638 in HEK293 cells and 515 in MEFs). Interestingly, many of these genes are involved in protein folding and nuclear transport (**Fig. 2c**). Using a firefly luciferase (Fluc) reporter containing the 5′ UTR, we validated the translational upregulation of nucleoporin-encoding gene *NUP88* (**Supplementary Fig. 7**). It is noteworthy that many starvation-responsive genes contain multiple TISs (1,286 in HEK293 cells and 1,343 in MEFs), which suggests a regulatory role for alternative TISs in translational control[21]. To demonstrate the influence of alternative translation on the aTIS initiation, we selected genes with multiple TISs and computed the ribosome density at the aTIS codon relative to the total TIS density on the same transcript (**Supplementary Fig. 8**). This analysis uncovered many genes whose translational regulation is indiscernible by simple comparison of ribosome density changes at either CDSs or aTISs. A total of 428 genes in HEK293 cells and 212 genes in MEFs demonstrated an altered aTIS-to-TIS ratio upon amino acid deprivation (false discovery rate <0.05). This strategy uncovered several stress-responsive genes whose transcripts contain previously uncharacterized TISs. For instance, *GADD45G* bears a CUG start codon in the 5′ UTR (**Fig. 2e**). Fluc reporter assays confirmed the critical role of 5′ UTR in the starvation-induced upregulation of *GADD45G* (**Fig. 2f**). In particular, deleting the CUG codon was sufficient to prevent the starvation responsiveness.

Programmatic TIS regulation in response to starvation

Many upstream open reading frames are believed to exert negative effects on the main open reading frame translation, presumably by capturing the scanning ribosome[12,22]. It is thus not surprising to find that a large number of multiple-TIS–containing genes showed increased aTIS initiation when uTIS initiation was repressed under starvation. However, a handful of transcripts exhibited decreased aTIS fraction despite the presence of alternative TISs (**Supplementary Fig. 8**). To identify possible factors governing differential regulation of alternative TISs, we surveyed for consensus sequence motifs in gene groups that respond differently to starvation. Among transcripts with increased aTIS initiation upon starvation, the Kozak consensus motif was prominent (**Supplementary Fig. 9a**). For transcripts with increased uTISs, an evident purine-rich sequence context emerged above the background (**Supplementary Fig. 9b**). This finding is reminiscent of the polypurine (A)-rich sequences found in many evolutionarily

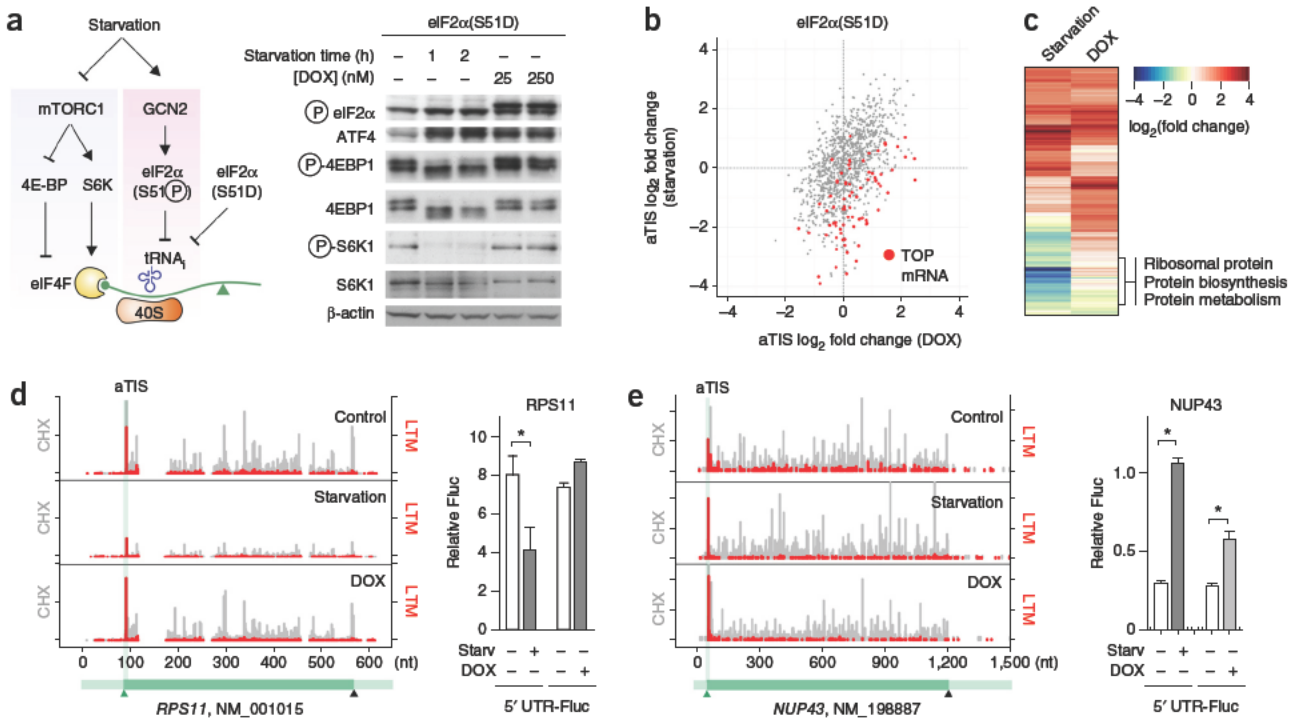

Figure 3 | Distinct role of eIF2α phosphorylation in translational response to starvation. (**a**) Left, schematic of mTORC1 signaling and eIF2α phosphorylation response. Right, immunoblotting results of eIF2α(S51D) mutant cells with either amino acid starvation or doxycycline (DOX)-induced eIF2α(S51D) expression. (**b**) Fold changes in LTM-associated aTIS density in eIF2α(S51D) mutant cells between amino acid starvation and DOX-induced eIF2α(S51D) expression. Terminal oligopyrimidine (TOP) mRNAs are shown as red dots. (**c**) Heat map of fold change of enriched GO terms ("Biological process") for gene groups with translational downregulation (blue) or upregulation (red) in response to amino acid starvation or DOX-induced eIF2α(S51D) expression. (**d**) Left, example of a gene (*RPS11*) showing translational repression in response to amino acid starvation but not DOX-induced eIF2α(S51D) expression. Right, validation of RPS11 translational control by a Fluc reporter bearing the 5′ UTR of *RPS11*. (**e**) Left, example of a gene (*NUP43*) showing translational upregulation in response to either amino acid starvation or DOX-induced eIF2α(S51D) expression. Right, validation of NUP43 translational control by a Fluc reporter bearing the 5′ UTR of *NUP43*. Data in **d**,**e** are mean ± s.e.m.; $n = 3$ biological replicates; $^*P < 0.01$ by Student's *t*-test.

conserved internal ribosome entry sites[23,24]. Alternatively, the purine-rich sequence may act in a manner opposite to the 5′ terminal oligopyrimidine (TOP) tract, whose translation is highly sensitive to the mTORC1 signaling pathway[25,26].

TIS regulation pathways in response to starvation

Amino acid deprivation suppresses global protein synthesis by inhibiting the mTORC1 signaling pathway and activating GCN2 kinases[27]. Whereas the former regulates cap recognition, the latter controls the ternary complex formation (**Fig. 3a**). It is unclear whether these distinct signaling pathways have overlapping or unique contributions to the translational regulation. We took advantage of a HEK293 cell line harboring an inducible phosphor-mimetic allele of eIF2α in which serine 51 was mutated to an aspartic acid (S51D)[28]. Expression of this mutant upon doxycycline (DOX) addition led to translational attenuation as well as an evident induction of ATF4 (**Fig. 3a** and **Supplementary Fig. 10a**). Unlike amino acid deprivation, however, eIF2α(S51D) expression had little effect on mTORC1 signaling (**Fig. 3a**). Therefore, the direct contribution of eIF2α phosphorylation to translational reprogramming can be dissected without pleiotropic effects caused by nutrient deprivation.

We applied QTI-seq to HEK293/eIF2α(S51D) cells with or without DOX treatment, together with RNA-seq and Ribo-seq. Similarly to amino acid starvation, eIF2α(S51D) expression resulted in evident differences for the LTM-associated aTIS ribosome density captured by QTI-seq (**Supplementary Fig. 10b** and **Supplementary Table 3**). A comparative analysis of the aTIS profiles between these two conditions revealed a partially overlapping gene pattern (**Fig. 3b**). Interestingly, the majority of overlapping genes were translationally upregulated with increased aTIS ribosome density. For those mRNAs undergoing translational repression under starvation, very few were affected in the presence of eIF2α(S51D), with the most notable gene group as TOP mRNAs (**Fig. 3b**). Clustering of the transcripts with changed aTIS ribosome density further confirmed the dichotomy of regulation between eIF2α(S51D) expression and starvation (**Fig. 3c**). In general, the transcripts commonly affected under both conditions were translationally upregulated and span diverse functions, whereas the starvation-sensitive mRNA subsets were translationally repressed and enriched in functions highly relevant to ribosome biogenesis. These results indicate that, in response to amino acid starvation, reduced mTORC1 signaling is more responsible for the suppression of TOP mRNA translation. In contrast, eIF2α phosphorylation contributes mainly to the selective upregulation of a subset of transcripts.

To confirm the differential regulation of translation initiation controlled by distinct upstream signaling pathways, we chose two genes for experimental validation. The gene encoding ribosomal protein RPS11 contains a typical TOP sequence on its 5′ UTR.

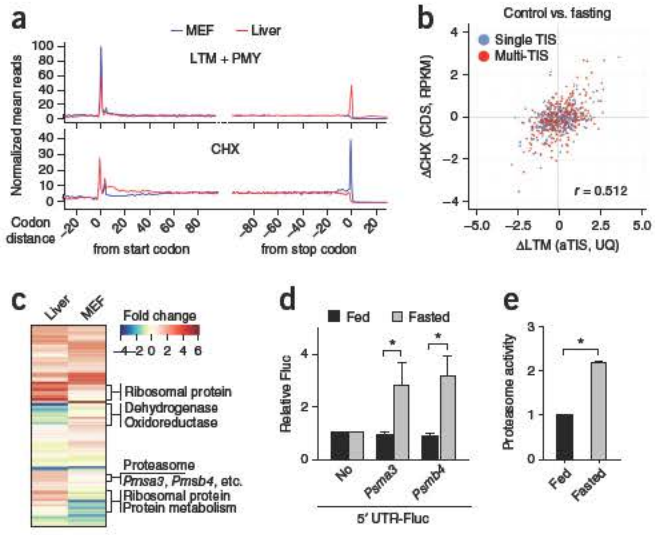

Figure 4 | Liver-specific QTI-seq reveals translational reprogramming in response to fasting. (**a**) Metagene analysis of LTM-associated ribosome density (top) or CHX-associated ribosome density (bottom) in MEFs and liver cells. Normalized RPF reads are averaged across the entire transcriptome and aligned at the annotated start codons and stop codons. (**b**) Fold changes in LTM-associated aTIS density and CHX-associated CDS ribosome occupancy in mouse liver cells with and without fasting. (**c**) Heat map of fold changes for gene groups with translational downregulation (blue) or upregulation (red) in liver cells of fasted mice or starved MEFs. (**d**) Reporter assay using an *in vitro* translation system reprogrammed from mouse liver lysates with or without fasting. The relative translation efficiency of a synthesized Fluc mRNA containing 5′ UTRs of *Psma3* or *Psmb4* is shown along with a no–5′ UTR condition. (**e**) Chymotrypsin activity of liver homogenates from mice 8–12 weeks old that were either fed or food deprived overnight, measured by Proteasome-Glo. Data in **d**,**e** are mean ± s.e.m.; $n = 3$ biological replicates; $^*P < 0.01$ by Student's *t*-test.

Amino acid starvation led to an approximately threefold decrease of the aTIS ribosome density (**Fig. 3d**). However, the translation of RPS11 exhibited little change in response to DOX-induced eIF2a(S51D) expression. The Fluc reporter bearing the *RPS11* 5′ UTR behaved exactly like the endogenous RPS11 in transfected cells (**Fig. 3d**). Amino acid starvation, but not eIF2a(S51D) expression, caused a significant reduction of Fluc expression. Unlike *RPS11*, the nucleoporin gene *NUP43* exhibited a translational upregulation after starvation or eIF2a(S51D) expression as evidenced by a more-than-threefold increase for its aTIS ribosome density (**Fig. 3e**). In agreement with the QTI-seq data, the Fluc reporter fused with the 5′ UTR of *NUP43* showed a consistent increase of translation in response to both conditions (**Fig. 3e**). These results strongly favor the hypothesis that distinct upstream signaling pathways act on different aspects of translation initiation, resulting in a coordinated translational reprogramming to achieve cellular adaptation.

Tissue-specific QTI-seq in liver cells

Having elucidated translational regulation from cells in culture, we reasoned that the principle of QTI-seq is applicable to solid tissues because it directly captures initiating ribosomes from lysates. To achieve cell type–specific ribosome profiling, we made use of the available RiboTag mouse, which carries a 'floxed' *Rpl22*^{HA} allele[13]. As a pilot study, we crossed the RiboTag mouse with a mouse expressing liver cell–specific Cre recombinase under the control of albumin promoter (Alb-Cre) (**Supplementary Fig. 11a**). The tissue specificity of Rpl22^{HA} incorporation into the ribosome was confirmed by anti-HA immunoprecipitation of polysome fractions (**Supplementary Fig. 11b**,**c**). In particular, the hepatocyte-specific transcripts were highly enriched in the tagged ribosome-associated mRNAs (**Supplementary Fig. 11d**). Following homogenization of liver tissues in the presence of LTM, PMY treatment led to efficient disassociation of the nonimmobilized ribosomes (**Supplementary Fig. 12a**). The LTM-preserved ribosome complexes bearing Rpl22^{HA} were enriched by anti-HA immunoprecipitation after RNase I digestion. Metagene analysis revealed an elevated ribosome density at the annotated start codon, a result suggesting that QTI-seq worked equally well in solid tissue samples (**Fig. 4a**). There were fewer TISs identified from liver cells than from MEFs (5,796 vs. 1,770), but they had a similar codon composition of TIS types (**Supplementary Fig. 13**). In addition, there was considerable overlap for the identified TISs between the two samples, and the overlap was further increased when we considered only the aTISs (**Supplementary Fig. 14**). The nonoverlapping TISs could be classified into differential aTISs and cell type–specific alternative TISs. For instance, the gene encoding hydroxyacyl-CoA dehydrogenase (HADH) showed a clear LTM peak at the aTIS in both liver and MEF samples (**Supplementary Fig. 15**). However, an in-frame downstream TIS was evident in the liver sample but vaguely present in the MEF sample. It is likely that liver cells can give rise to different isoforms of HADH enzyme.

Liver-specific TIS profile in response to fasting

The successful application of QTI-seq in mouse liver offers a unique opportunity to explore the translational response to a fasting condition at the organismal level. To this end, liver-specific RiboTag mice were subject to overnight fasting followed by RNA-seq, Ribo-seq and QTI-seq. Food deprivation resulted in large disassembly of polysomes in liver tissues (**Supplementary Fig. 12a**). Consistently, liver-specific QTI-seq uncovered extensive changes of ribosome density at the aTISs (**Supplementary Fig. 12b** and **Supplementary Table 4**). Supporting the quantitative feature of liver-specific QTI-seq, the changes of aTIS ribosome density in response to fasting correlated well with the differences of CDS ribosome occupancy ($r = 0.512$; **Fig. 4b**). Interestingly, overnight fasting elicited distinct translational responses in liver cells when compared to MEFs under starvation (**Fig. 4c**). Although MEFs showed prominent repression of ribosome biogenesis in response to starvation, this negative translational response was no longer obvious in liver cells after overnight fasting. In fact, some ribosomal protein genes underwent translational upregulation in fasted liver. This observation suggests that, contrary to the widely accepted notion, global inhibition of the translation machinery is a transient response upon acute nutrient deprivation. Under prolonged fasting conditions, a continuous supply of ribosomal proteins is likely needed for selective protein synthesis.

Many of the transcripts showing higher aTIS ribosome density encode components of the protein degradation pathway, in particular the proteasome system (**Fig. 4c**). This is consistent with the finding that the ubiquitin-proteasome system not only helps to remove misfolded or damaged proteins[29] but also contributes to intracellular amino acid recycling during nutrient deprivation[30].

Our results—for the first time, to our knowledge—demonstrate a translational mechanism that promotes the proteasome activity in response to prolonged fasting. To obtain direct evidence for translational control of the proteasome system, we cloned the 5′ UTR of several proteasome genes and fused them to the Fluc reporter. We established a reconstituted translation system programmed from the liver homogenates to mimic the *in vivo* translation environment. Using equal amounts of synthesized mRNAs, we found that the presence of 5′ UTR of *Psma3* or *Psmb4* resulted in a greater-than-threefold increase of Fluc activity in liver cells obtained from fasted mice but not in liver cells from normally fed mice (**Fig. 4d**). To ascertain the functional consequence of this translational switch in response to fasting, we directly measured the proteasome activity in liver homogenates using Proteasome-Glo. Overnight fasting resulted in a more-than-twofold increase in the proteasome chymotrypsin activity (**Fig. 4e**). Our results indicate a coordinated regulation between protein synthesis and degradation, which provides an elegant mechanism for cells and tissues to achieve metabolic homeostasis under nutrient deprivation.

DISCUSSION

Translation initiation is a crucial point of regulation in eukaryotic gene expression, allowing cells to adapt rapidly to changing environmental conditions[4–7]. The significance of translation initiation is further substantiated by the existence of alternative translation that utilizes one or more potential TISs in addition to the main start codon[12]. The ability to monitor quantitatively the engagement of 80S ribosomes at the individual TIS would provide an effective means to evaluate start codon selection and to uncover fundamental principles underlying translational regulation. Compared to GTI-seq, which we developed previously[15], QTI-seq represents a conceptually distinct approach that permits quantitative profiling of initiating ribosomes in samples from cells in culture and solid tissues.

The applicability of QTI-seq to solid tissues has the potential to greatly advance our understanding of the basic mechanisms of translation initiation from cellular to organismal levels. Using RiboTag mice, we demonstrated liver cell–specific profiling of initiating ribosomes. This can serve as a prototype for tissue-specific ribosome profiling using other techniques such as bacTRAP[14]. QTI-seq revealed that after overnight fasting, liver cells had a pattern of translational response distinct from that of MEFs under acute starvation, as follows. First, the global reduction of TOP mRNA translation was no longer evident, which suggests that a continuous supply of ribosomal proteins is needed for selective protein synthesis. Second, QTI-seq uncovered a potent translational reprogramming for the proteasome system. The ubiquitin-proteasome system targets many proteins for degradation, and the lethality of proteasome inhibition has been attributed to amino acid scarcity[31]. It therefore makes intuitive sense that the upregulation of the proteasome system is essential for cell survival so as to continuously supply amino acids. It will be of much interest to demonstrate this phenomenon in other types of tissues, such as skeletal muscle, in response to fasting.

METHODS

Methods and any associated references are available in the online version of the paper.

Accession codes. NCBI Sequence Read Archive: raw sequence data have been deposited under accession SRA160745.

Note: Any Supplementary Information and Source Data files are available in the online version of the paper.

ACKNOWLEDGMENTS

We thank the Qian lab members for helpful discussion; J. Parker and R. Weiss for critical reading of the manuscript; P. Walter (University of California at San Francisco) for the eIF2α(S51D) cell line; and Cornell University Life Sciences Core Laboratory Center for performing deep sequencing. This work was supported by grants to B.S. from the US National Institutes of Health (NIH CA106150) and to S.-B.Q. from the NIH (DP2 OD006449, R01AG042400), Ellison Medical Foundation (AG-NS-0605-09) and US Department of Defense (W81XWH-14-1-0068).

AUTHOR CONTRIBUTIONS

X.G. and S.-B.Q. conceived of the original idea. X.G. designed experimental approaches and performed the experiments. J.W. analyzed the data. B.L. assisted data interpretation. M.M. and B.S. synthesized LTM. S.-B.Q. wrote the paper.

COMPETING FINANCIAL INTERESTS

The authors declare no competing financial interests.

1. Aitken, C.E. & Lorsch, J.R. A mechanistic overview of translation initiation in eukaryotes. *Nat. Struct. Mol. Biol.* **19**, 568–576 (2012).
2. Gray, N.K. & Wickens, M. Control of translation initiation in animals. *Annu. Rev. Cell Dev. Biol.* **14**, 399–458 (1998).
3. Gebauer, F. & Hentze, M.W. Molecular mechanisms of translational control. *Nat. Rev. Mol. Cell Biol.* **5**, 827–835 (2004).
4. Sonenberg, N. & Hinnebusch, A.G. Regulation of translation initiation in eukaryotes: mechanisms and biological targets. *Cell* **136**, 731–745 (2009).
5. Spriggs, K.A., Bushell, M. & Willis, A.E. Translational regulation of gene expression during conditions of cell stress. *Mol. Cell* **40**, 228–237 (2010).
6. Liu, B. & Qian, S.B. Translational reprogramming in cellular stress response. *Wiley Interdiscip. Rev. RNA* **5**, 301–315 (2014).
7. Jackson, R.J., Hellen, C.U. & Pestova, T.V. The mechanism of eukaryotic translation initiation and principles of its regulation. *Nat. Rev. Mol. Cell Biol.* **11**, 113–127 (2010).
8. Ingolia, N.T., Ghaemmaghami, S., Newman, J.R. & Weissman, J.S. Genome-wide analysis *in vivo* of translation with nucleotide resolution using ribosome profiling. *Science* **324**, 218–223 (2009).
9. Ingolia, N.T. Ribosome profiling: new views of translation, from single codons to genome scale. *Nat. Rev. Genet.* **15**, 205–213 (2014).
10. Plotkin, J.B. & Kudla, G. Synonymous but not the same: the causes and consequences of codon bias. *Nat. Rev. Genet.* **12**, 32–42 (2011).
11. Shah, P., Ding, Y., Niemczyk, M., Kudla, G. & Plotkin, J.B. Rate-limiting steps in yeast protein translation. *Cell* **153**, 1589–1601 (2013).
12. Morris, D.R. & Geballe, A.P. Upstream open reading frames as regulators of mRNA translation. *Mol. Cell. Biol.* **20**, 8635–8642 (2000).
13. Sanz, E. *et al.* Cell-type-specific isolation of ribosome-associated mRNA from complex tissues. *Proc. Natl. Acad. Sci. USA* **106**, 13939–13944 (2009).
14. Heiman, M. *et al.* A translational profiling approach for the molecular characterization of CNS cell types. *Cell* **135**, 738–748 (2008).
15. Lee, S., Liu, B., Huang, S.X., Shen, B. & Qian, S.B. Global mapping of translation initiation sites in mammalian cells at single-nucleotide resolution. *Proc. Natl. Acad. Sci. USA* **109**, E2424–E2432 (2012).
16. Schneider-Poetsch, T. *et al.* Inhibition of eukaryotic translation elongation by cycloheximide and lactimidomycin. *Nat. Chem. Biol.* **6**, 209–217 (2010).
17. Fritsch, C. *et al.* Genome-wide search for novel human uORFs and N-terminal protein extensions using ribosomal footprinting. *Genome Res.* **22**, 2208–2218 (2012).
18. Blobel, G. & Sabatini, D. Dissociation of mammalian polyribosomes into subunits by puromycin. *Proc. Natl. Acad. Sci. USA* **68**, 390–394 (1971).
19. David, A. *et al.* Nuclear translation visualized by ribosome-bound nascent chain puromycylation. *J. Cell Biol.* **197**, 45–57 (2012).
20. Ingolia, N.T., Lareau, L.F. & Weissman, J.S. Ribosome profiling of mouse embryonic stem cells reveals the complexity and dynamics of mammalian proteomes. *Cell* **147**, 789–802 (2011).

21. Calvo, S.E., Pagliarini, D.J. & Mootha, V.K. Upstream open reading frames cause widespread reduction of protein expression and are polymorphic among humans. *Proc. Natl. Acad. Sci. USA* **106**, 7507–7512 (2009).
22. Kozak, M. Pushing the limits of the scanning mechanism for initiation of translation. *Gene* **299**, 1–34 (2002).
23. Dorokhov, Y.L. *et al.* Polypurine (A)-rich sequences promote cross-kingdom conservation of internal ribosome entry. *Proc. Natl. Acad. Sci. USA* **99**, 5301–5306 (2002).
24. Gilbert, W.V., Zhou, K., Butler, T.K. & Doudna, J.A. Cap-independent translation is required for starvation-induced differentiation in yeast. *Science* **317**, 1224–1227 (2007).
25. Meyuhas, O. Synthesis of the translational apparatus is regulated at the translational level. *Eur. J. Biochem.* **267**, 6321–6330 (2000).
26. Hamilton, T.L., Stoneley, M., Spriggs, K.A. & Bushell, M. TOPs and their regulation. *Biochem. Soc. Trans.* **34**, 12–16 (2006).
27. Hinnebusch, A.G. Translational regulation of GCN4 and the general amino acid control of yeast. *Annu. Rev. Microbiol.* **59**, 407–450 (2005).
28. Sidrauski, C. *et al.* Pharmacological brake-release of mRNA translation enhances cognitive memory. *Elife* **2**, e00498 (2013).
29. Sherman, M.Y. & Goldberg, A.L. Cellular defenses against unfolded proteins: a cell biologist thinks about neurodegenerative diseases. *Neuron* **29**, 15–32 (2001).
30. Vabulas, R.M. & Hartl, F.U. Protein synthesis upon acute nutrient restriction relies on proteasome function. *Science* **310**, 1960–1963 (2005).
31. Suraweera, A., Munch, C., Hanssum, A. & Bertolotti, A. Failure of amino acid homeostasis causes cell death following proteasome inhibition. *Mol. Cell* **48**, 242–253 (2012).

nature structural & molecular biology

Translational control of the cytosolic stress response by mitochondrial ribosomal protein L18

Xingqian Zhang[1], Xiangwei Gao[1,4], Ryan Alex Coots[1,2], Crystal S Conn[3], Botao Liu[3] & Shu-Bing Qian[1–3]

In response to stress, cells attenuate global protein synthesis but permit efficient translation of mRNAs encoding heat-shock proteins (HSPs). Although decades have passed since the first description of the heat-shock response, how cells achieve translational control of HSP synthesis remains enigmatic. Here we report an unexpected role for mitochondrial ribosomal protein L18 (MRPL18) in the mammalian cytosolic stress response. MRPL18 bears a downstream CUG start codon and generates a cytosolic isoform in a stress-dependent manner. Cytosolic MRPL18 incorporates into the 80S ribosome and facilitates ribosome engagement on mRNAs selected for translation during stress. MRPL18 knockdown has minimal effects on mitochondrial function but substantially dampens cytosolic HSP expression at the level of translation. Our results uncover a hitherto-uncharacterized stress-adaptation mechanism in mammalian cells, which involves formation of a 'hybrid' ribosome responsible for translational regulation during the cytosolic stress response.

Cell survival in a changing environment requires swift regulation of gene expression, including translational control of existing mRNAs[1]. Global translation is generally suppressed in response to most, if not all, types of cellular stress[2,3]. However, subsets of transcripts undergo selective translation to produce proteins that are vital for cell survival and stress recovery. One of the best-known examples is the heat-shock protein 70 (Hsp70), whose synthesis is upregulated in cells upon elevated temperatures or exposure to proteotoxic stress[4,5]. Although transcriptional regulation after heat shock is well characterized[6,7], understanding of how efficient synthesis of HSPs persists when the translation machinery is generally compromised has remained elusive. It is commonly believed that the 5′ untranslated region (5′ UTR) of Hsp70 mRNA recruits the translational apparatus in a cap-independent manner[8–11]. However, neither the specific translation-promoting features of Hsp70 mRNAs nor the regulatory mechanism of the translation machinery has been clearly defined. In particular, it is unknown whether specialized ribosomes are required for efficient Hsp70 synthesis under stress conditions.

The ribosome is a large ribonucleoprotein complex composed of two subunits that associate upon the initiation of translation[12]. The small subunit decodes mRNA, and the large subunit catalyzes peptide-bond formation. In mammalian cells, there are two sets of ribosome particles, which reside in the cytoplasm and the mitochondria. Although ribosomal proteins (RPs) are all synthesized in the cytoplasm, they assemble into functional subunits in different subcellular compartments[13]. The mitochondrial RPs (MRPs) are encoded by nuclear genes, are synthesized in the cytosol and are then imported into mitochondria for assembly; they are responsible for translation of 13 mitochondrial mRNAs[14]. In contrast, cytosolic ribosomes are assembled within the nucleolus and are then exported into the cytoplasm for mRNA translation. Because of their distinct composition and cellular localization, there is believed to be little functional connection between mitochondrial and cytosolic ribosomes.

Here we set out to investigate whether specialized ribosomes are required in the cytosolic stress response. We report that MRPL18 bears a hidden CUG start codon downstream of the main initiation site. Stress conditions such as heat shock trigger CUG-initiated alternative translation, to generate a cytosolic isoform of MRPL18. We found that the cytosolic MRPL18 integrates into the 80S ribosome complex in a stress-dependent manner and facilitates synthesis of stress proteins such as Hsp70. Our results uncover a hitherto-uncharacterized stress-adaptation mechanism in mammalian cells, which involves formation of a hybrid ribosome that promotes synthesis of stress proteins.

RESULTS

MRPL18 alternative translation produces a cytosolic isoform

We used our previously developed approach, global translation initiation sequencing (GTI-seq), which allows precise mapping of alternative translation initiation sites (TISs) across the entire transcriptome[15]. The transcript encoding MRPL18 bears several interesting features. First, MRPL18 shows three TISs, with the annotated start codon (aTIS) flanked by an upstream TIS (uTIS) and a downstream TIS (dTIS) (**Fig. 1a**). Whereas the uTIS codon is an AUG, the dTIS uses CUG as the initiator. Intriguingly, the CUG initiator is located immediately after the predicted mitochondrial targeting signal (MTS) of MRPL18 and within the same reading frame. It is likely that CUG-initiated translation produces a cytosolic isoform of MRPL18. However, the identical size of cytosolic MRPL18 (MRPL18(cyto))

[1]Division of Nutritional Sciences, Cornell University, Ithaca, New York, USA. [2]Graduate Field of Nutritional Sciences, Cornell University, Ithaca, New York, USA. [3]Graduate Field of Genetics, Genomics and Development, Cornell University, Ithaca, New York, USA. [4]Present address: Institute of Environmental Medicine, Zhejinag University School of Medicine, Hangzhou, People's Republic of China. Correspondence should be addressed to S.-B.Q. (sq38@cornell.edu).

Received 21 November 2014; accepted 13 March 2015; published online 13 April 2015; doi:10.1038/nsmb.3010

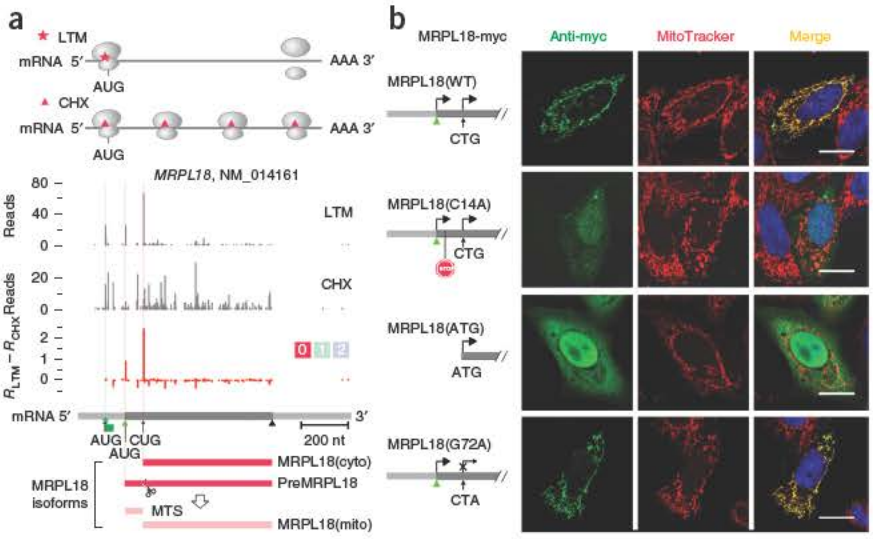

Figure 1 MRPL18 undergoes alternative translation to produce a cytosolic isoform. (**a**) Top, schematic of GTI-seq with translation inhibitors lactimidomycin (LTM) and cycloheximide (CHX). Raw read counts per nucleotide position of *MRPL18* are plotted as a bar graph. Middle, processed LTM read density (*R*), color-coded by the corresponding reading frame, with the identified TIS positions marked by asterisks. Bottom, predicted isoforms of MRPL18. (**b**) Immunostaining of HeLa cells transfected with MRPL18 wild type and mutants illustrated at left. Anti-myc is shown in the green channel and MitoTracker in the red channel. 4′,6-diamidino-2-phenylindole (DAPI) was used for nuclear counterstaining. Scale bars, 10 μm.

and the MTS-cleaved mitochondrial MRPL18 (MRPL18(mito)) renders them indistinguishable by standard immunoblotting.

To experimentally confirm the alternative translation of MRPL18, we constructed a series of MRPL18 mutants bearing myc tags and examined their subcellular localization in HeLa cells. The wild-type MRPL18 was mostly localized in mitochondria, as revealed by immunofluorescence staining (**Fig. 1b**). The vague cytoplasmic staining suggests that the CUG-initiated MRPL18(cyto) was not a major product under the normal growth condition. To show exclusively the CUG-initiated translation, we created a stop codon between the aTIS and the dTIS to prevent the synthesis of full-length MRPL18. This mutant, MRPL18(C14A), exhibited a clear localization in the cytosol and the nucleus (**Fig. 1b**). We saw a similar pattern for MRPL18(ATG), a truncated version of MRPL18 lacking both the 5′ UTR and the MTS. In contrast, MRPL18(G72A), a mutant with the dTIS mutated to CTA, showed a predominant mitochondrial localization. Together, these results indicate that MRPL18 bears a hidden downstream CUG start codon whose initiation gives rise to a cytosolic isoform of MRPL18.

MRPL18 undergoes stress-induced alternative translation

Notably, the CUG-only MRPL18(C14A) had much lower expression levels than other transgenes (**Fig. 1b** and **Supplementary Fig. 1a**), a result suggesting that the downstream CUG initiator is less efficient than the authentic AUG start codon. Interestingly, *Mrpl18* is a heat shock–responsive gene[16], and a recent study indicated that *MRPL18* is one of the direct targets of heat-shock transcription factor 1 (HSF1)[17]. Using a mouse fibroblast cell line lacking HSF1 (ref. 18), we confirmed the transcriptional upregulation of *Mrpl18* upon heat shock (**Supplementary Fig. 1b**). To investigate whether MRPL18 undergoes translational regulation in response to stress, we compared the abundance of transfected MRPL18 mutants in HeLa cells before and after heat shock. These transgenes maintained similar mRNA levels in response to heat shock (**Supplementary Fig. 1c**), thus allowing direct evaluation of translational control. Immunoblotting showed two bands of transfected MRPL18, corresponding to the MRPL18 precursor and the MRPL18 species lacking the MTS (**Fig. 2a**, lane 3). The transfected MRPL18 undergoes less efficient processing than the endogenous counterpart, presumably owing to reduced mitochondrial import because the transgene lacks the 3′ untranslated region (3′ UTR) of MRPL18 (ref. 19). As expected, the imported exogenous MRPL18 incorporated into mitochondrial ribosomes, as evidenced by its cosedimentation with other mitoribosomal proteins (**Supplementary Fig. 1d**). Upon heat-shock stress, the full-length wild-type MRPL18 (MRPL18(WT)) showed a modest increase, whereas we observed much less change for MRPL18(ATG), which lacks both the 5′ UTR and the MTS region (**Fig. 2a**, lanes 9 and 10). Remarkably, the CUG-only MRPL18(C14A) exhibited the strongest responsiveness despite its low basal levels in cells without stress (**Fig. 2a**, lanes 7 and 8). To substantiate this finding further, we constructed reporters by replacing the main coding region of MRPL18 with firefly luciferase (Fluc). Consistently with the immunoblotting results of MRPL18 mutants, the chimeric C14A-Fluc exhibited the highest increase of Fluc expression in response to heat-shock stress (**Fig. 2b**).

Having confirmed the stress-induced alternative translation of MRPL18 by using mutants, we next sought to determine whether MRPL18(WT) undergoes a translational switch from the authentic AUG to the downstream CUG in response to heat-shock stress. It is challenging to unequivocally monitor the newly synthesized MRPL18(cyto) because of the high basal levels of MRPL18(mito) present in cells before stress. To circumvent this limitation, we engineered a reversible destabilization domain (DD) by fusing it to the COOH terminus of MRPL18(WT) (**Fig. 2c**). This system permits temporal examination of newly synthesized MRPL18-DD after addition of Shield-1, a cell-permeable drug that binds the DD to protect the protein from degradation[20]. HeLa cells transfected with plasmids expressing MRPL18-DD exhibited minimal anti-myc signals in the absence of Shield-1 (**Supplementary Fig. 2a**). Treatment with Shield-1 stabilized MRPL18-DD, which had a clear mitochondrial localization (**Fig. 2c** and **Supplementary Fig. 2b**). Remarkably, heat-shock stress before Shield-1 addition resulted in substantial anti-myc signals in the cytosol as well as the nucleus (**Fig. 2c** and **Supplementary Fig. 2c**). This observation was not due to mitochondrion leakage, because the stress-induced Hsp60 remained exclusively in mitochondria after heat shock. This result confirms that heat-shock stress triggers CUG-mediated alternative translation within the wild-type sequence context of MRPL18.

MRPL18(cyto) is dependent on eIF2α phosphorylation

What is the mechanism underlying stress-induced alternative translation of MRPL18? We looked into eukaryotic initiation factor 2α (eIF2α), whose phosphorylation regulates ATF4, in a classical example of alternative translation triggered by many stress conditions[21–24]. Consistently with a previous report[25], heat-shock stress also triggered eIF2α phosphorylation (**Supplementary Fig. 3a**). To address the role of eIF2α phosphorylation in the alternative translation of MRPL18, we transfected MRPL18-Fluc reporters into a mouse embryonic fibroblast (MEF) cell line bearing a nonphosphorylatable eIF2α in which

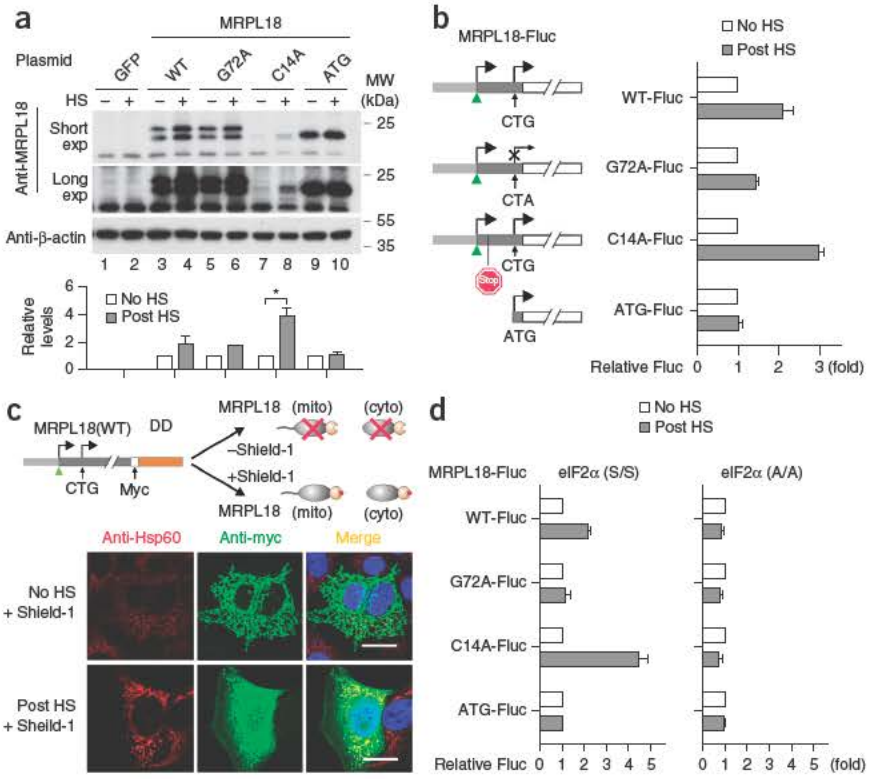

Figure 2 MRPL18 undergoes alternative translation in a stress-dependent manner. (**a**) Representative immunoblot results of HeLa cells transfected with the indicated plasmids and collected before heat shock (HS) or 2.5 h after heat shock (43 °C, 1 h). Top bands are uncleaved MRPL18 precursors. β-actin is a loading control. The bottom graph shows the relative levels of transgenes (small isoform) normalized to β-actin. Error bars, s.e.m. ($n = 3$ cell cultures, $^*P < 0.01$ by two-tailed Student's t test). MW, molecular weight; exp, exposure. (**b**) Fluc reporter assays in HeLa cells transfected with MRPL18-Fluc constructs shown at left. Fluc activities after heat shock are normalized to those in nonstressed cells. Error bars, s.e.m. ($n = 3$ cell cultures). (**c**) Immunostaining of HeLa cells transfected with MRPL18-DD with or without heat shock in the presence of Shield-1. Anti-Hsp60 antibody is shown in the red channel and anti-myc in the green channel. Scale bars, 10 μm. A schematic of MRPL18-DD fusion protein in the absence or presence of Shield-1 is shown at top. (**d**) Fluc reporter assays in eIF2α (S/S) and eIF2α (A/A) MEFs transfected with MRPL18-Fluc constructs shown in **b**. Fluc activities after heat shock are normalized to those of nonstressed cells. Error bars, s.e.m. ($n = 3$ cell cultures). Original blot images are in **Supplementary Data Set 1**.

Ser51 (S/S genotype) was mutated to an alanine (A/A genotype)[26]. As expected, wild-type MEF (S/S) cells showed a similar pattern of Fluc expression as HeLa cells (**Fig. 2d**). In particular, the CUG-only MRPL18(C14A) exhibited the highest increase of Fluc (more than four-fold) in response to heat-shock stress, whereas the expression level of the AUG-only MRPL18(G72A) remained unchanged. Remarkably, the stress responsiveness of MRPL18(C14A) was completely abolished in MEF (A/A) cells (**Fig. 2d** and **Supplementary Fig. 3b**), thus indicating that the alternative translation of MRPL18 is dependent on eIF2α phosphorylation.

MRPL18(cyto) integrates into cytosolic 80S ribosomes

Given that the authentic role of MRPL18 is to constitute the ribosome complex within mitochondria, we speculated that MRPL18(cyto) may integrate into the cytosolic 80S ribosome complex under stress conditions. To test this hypothesis, we assessed the behavior of endogenous MRPL18 as well as transfected mutants in HeLa cells. We first purified cytosolic ribosome complexes with affinity immunoprecipitation (IP) in order to eliminate mitochondrial ribosome contamination. We also converted the polysomes into monosomes by RNase I digestion before IP to exclude indirect pulldown of RNA-binding proteins (**Fig. 3a**). Endogenous MRPL18, but not other mitochondrial proteins, was readily precipitated from stressed cells by either anti-RPL4 or anti-RPS6 antibodies (**Fig. 3a**, lanes 2 and 6). In addition, we recovered endogenous MRPL18 from the polysome fraction after heat-shock stress and found that this redistribution was sensitive to the translation inhibitor cycloheximide (CHX) (**Supplementary Fig. 4**). Therefore, the cytosolic ribosome-associated MRPL18 is newly synthesized after

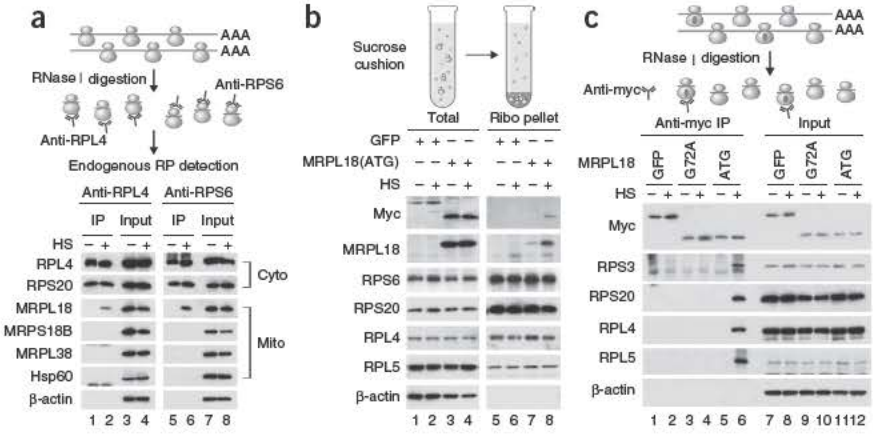

Figure 3 Cytosolic MRPL18 incorporates into the 80S ribosome in a stress-dependent manner. (**a**) Detection of MRPL18 in endogenous ribosomes purified from HeLa cells with or without heat shock. Immunoblotting of RNase I–digested cell lysates immunoprecipitated with anti-RPL4 (left) or anti-RPS6 (right) antibodies. Input and immunoprecipitates (IP) are indicated. Cyto, cytoplasmic; mito, mitochondrial. (**b**) Immunoblot detection of myc-tagged MRPL18(ATG) from endogenous ribosomes isolated by sucrose cushion from HeLa cells with or without heat shock. HeLa cells transfected with GFP are a control. Total lysate and ribosome (ribo) pellet are indicated. (**c**) Immunoblot detection of cytosolic ribosomal proteins from anti-myc immunoprecipitates. Samples are HeLa cells transfected with myc-tagged MRPL18(ATG), with or without heat shock, and HeLa cells transfected with GFP and MRPL18(G72A) as controls. Cell lysates were treated with RNase I before anti-myc IP. Throughout figure, β-actin is a loading control. Experiment schematics are shown at top. Original blot images are in **Supplementary Data Set 1**.

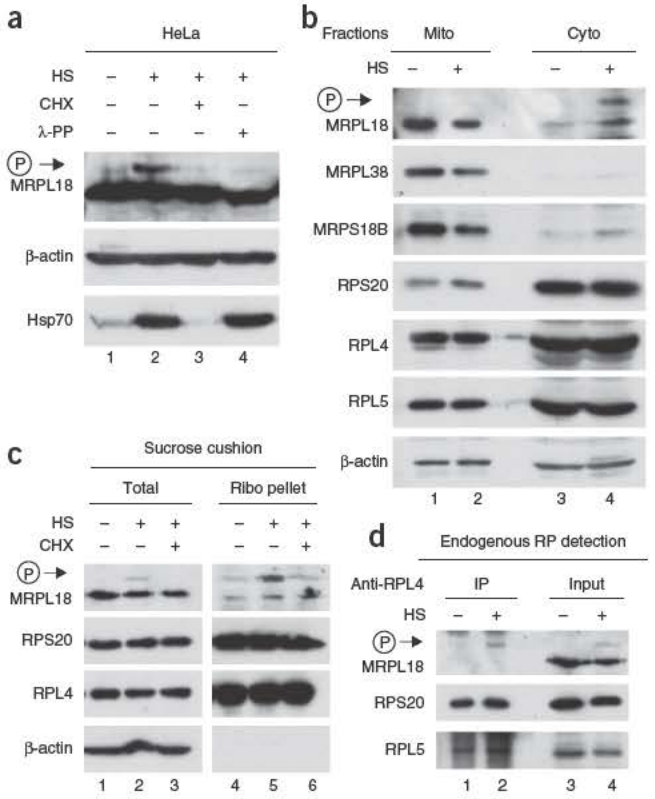

Figure 4 Cytosolic MRPL18 incorporates into the 80S ribosome in a phosphorylation-dependent manner. (**a**) Detection of phosphorylated MRPL18 in HeLa cells with or without heat-shock stress. Immunoblotting of whole cell lysates with or without λ-phosphatase (λ-PP) treatment, separated with Phos-tag acrylamide gel (MRPL18 only) or standard PAGE. CHX treatment during heat shock was included to demonstrate phosphorylation of newly synthesized MRPL18. (**b**) Detection of phosphorylated (P) MRPL18 in HeLa cell fractions with or without heat-shock stress. Immunoblotting of HeLa lysates with or without heat shock, fractionated with a mitochondria fractionation kit and separated with Phos-tag acrylamide gel (MRPL18 only) or standard PAGE. (**c**) Detection of phosphorylated MRPL18 in ribosome fractions of HeLa cells with or without heat-shock stress. Immunoblotting of total lysate and ribosome fractions prepared by sucrose cushion, separated with Phos-tag acrylamide gel (MRPL18 only) or standard PAGE. (**d**) Detection of phosphorylated MRPL18 in ribosomes purified from HeLa cells with or without heat-shock stress. Immunoblotting of RNase I–digested total lysates and anti-RPL4 immunoprecipitates, separated with Phos-tag acrylamide gel (MRPL18 only) or standard PAGE. Throughout figure, β-actin is a loading control. Original blot images are in **Supplementary Data Set 1**.

stress. We further confirmed the incorporation of MRPL18(cyto) into the 80S ribosome complex by using transfected MRPL18(ATG). Both cosedimentation binding analysis and anti-myc IP revealed a robust association of MRPL18(ATG) with cytosolic ribosomes in a stress-dependent manner (**Fig. 3b**, lane 8 and **Fig. 3c**, lane 6). In contrast, the AUG-only MRPL18(G72A) did not coprecipitate with any cytosolic RPs before or after heat-shock stress (**Fig. 3c**).

Phosphorylated MRPL18(cyto) integrates into 80S ribosomes

Interestingly, very little transfected MRPL18(ATG) was associated with the 80S ribosome in unstressed cells in spite of comparable expression levels. To investigate the mechanism of stress-induced incorporation, we examined the phosphorylation status of MRPL18 by using a Phos-tag acrylamide gel. An MRPL18 band with slower migration was clearly discernible upon heat-shock stress, and it was sensitive to phosphatase treatment (**Fig. 4a**). Addition of the translation inhibitor CHX completely abolished this species, thus suggesting that newly synthesized MRPL18 is phosphorylated during stress. Importantly, we found the phosphorylated MRPL18 exclusively in the cytosolic fraction (**Fig. 4b**), and we recovered only the phosphorylated species from the cytosolic 80S ribosome (**Fig. 4c,d**). We next searched for the kinase responsible for MRPL18 phosphorylation. Interestingly, MRPL18 was predicted to be a substrate of the tyrosine protein kinase Lyn[27]. Indeed, both the Lyn-specific chemical inhibitor bafetinib (**Fig. 5a**) and small hairpin RNA (shRNA)-mediated knockdown of Lyn (**Fig. 5b**) reduced the phosphorylation level of MRPL18. Notably, Lyn is a member of the Src family, whose kinase activity is increased upon heat-shock stress[28]. These results collectively indicate that both the production and function of MRPL18(cyto) are under tight control in response to stress.

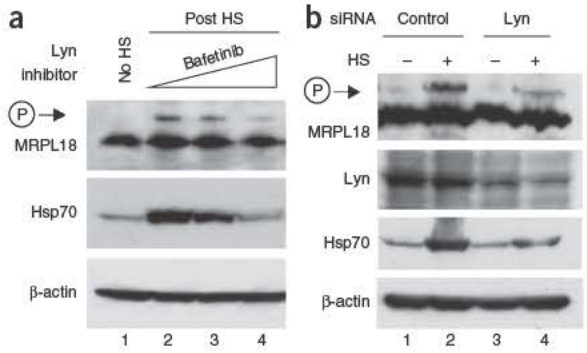

Figure 5 Cytosolic MRPL18 undergoes Lyn-mediated phosphorylation. (**a**) Detection of phosphorylated MRPL18 in HeLa cells in the presence of increasing doses of bafetinib immediately after heat-shock stress. Immunoblotting of whole cell lysates separated with Phos-tag acrylamide gel (MRPL18 only) or standard PAGE. (**b**) Detection of phosphorylated MRPL18 in HeLa cells transfected with SMARTpool siRNAs targeting Lyn or control shRNA targeting scrambled sequences. Immunoblotting of whole cell lysates separated with Phos-tag acrylamide gel (MRPL18 only) or standard PAGE. Throughout figure, β-actin is a loading control. Original blot images are in **Supplementary Data Set 1**.

MRPL18(cyto) promotes stress-protein synthesis during stress

The stress-inducible feature of MRPL18(cyto) is suggestive of its regulatory role in the cytosolic stress response. To elucidate its physiological function, we knocked down MRPL18 in HeLa cells with SMARTpool small interfering RNAs (siRNAs). Reduction in MRPL18 expression had minimal effects on cell growth and did not alter the rate of global protein synthesis (**Supplementary Fig. 5a**). In addition, we observed minimal effects of MRPL18 depletion on mitochondrial translation after short-term siRNA knockdown or long-term lentivirus-based shRNA knockdown (**Supplementary Fig. 5b,c**). However, upon heat-shock treatment, the induction of Hsp70 expression in the cytosol was largely dampened in cells with MRPL18 knockdown compared to cells transfected with control siRNA (**Fig. 6a**). To substantiate this finding further, we applied shRNA to HeLa cells and MEFs (**Fig. 6b** and **Supplementary Fig. 6**). shRNA-mediated MRPL18 knockdown resulted in impaired Hsp70 induction in both cells after heat-shock stress. This result was not due to transcriptional deficiency of Hsp70 gene expression. In fact, MEFs with MRPL18 knockdown demonstrated even higher Hsp70 transcript levels than the control cells in response to heat-shock stress (**Supplementary Fig. 6d**).

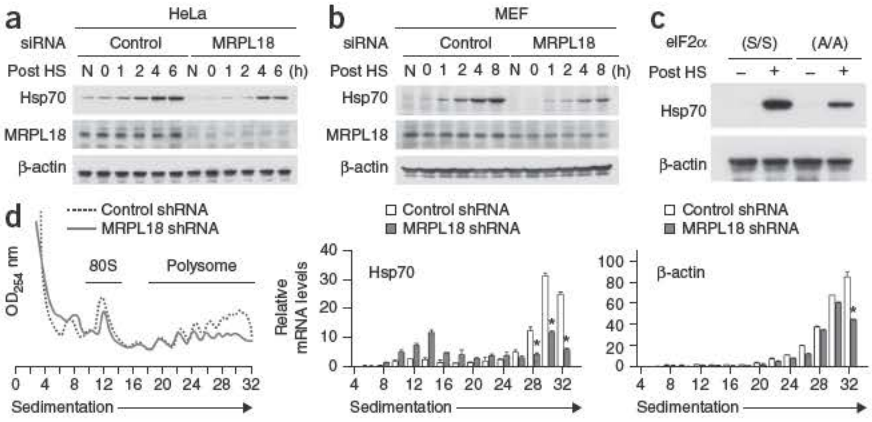

Figure 6 Cytosolic MRPL18 promotes Hsp70 biosynthesis after heat-shock stress. (**a**) Examination of heat shock–induced Hsp70 synthesis in HeLa cells transfected with SMARTpool siRNAs targeting MRPL18 or control shRNA targeting scrambled sequences. Immunoblotting of cell lysates collected at indicated times after heat shock. N, no heat shock. (**b**) Examination of heat shock–induced Hsp70 synthesis in MEFs infected with lentiviruses expressing shRNAs targeting MRPL18 or control shRNA. Immunoblotting of cell lysates collected at the indicated times after heat shock. (**c**) Examination of heat shock–induced Hsp70 synthesis in eIF2α (S/S) and eIF2α (A/A) MEFs after heat-shock stress. (**d**) Examination of polysome-enriched Hsp70 mRNA in MEFs infected with lentiviruses expressing shRNA targeting MRPL18 or control shRNA. Quantitative PCR measuring Hsp70 and β-actin mRNA levels in total RNA extracted from polysome fractions. Relative levels are normalized to the total. OD_{254}, optical density at 254 nm. Error bars, s.e.m. ($n = 3$ cell cultures, $^*P < 0.05$ by two-tailed Student's t test). Throughout figure, β-actin is a loading control. Original blot images are in **Supplementary Data Set 1**.

Given that the *de novo* synthesis of MRPL18(cyto) relies on alternative translation, we reasoned that suppressing CUG initiation would have a similar effect as MRPL18 knockdown. Indeed, stress-induced Hsp70 synthesis was substantially reduced in eIF2α (A/A) cells, whose eIF2α is not phosphorylatable (**Fig. 6c**). Because the incorporation of MRPL18(cyto) into the 80S ribosome is phosphorylation dependent, we examined the effects of reduced Lyn kinase activities in the stress response. Treatment with the Lyn inhibitor bafetinib or Lyn knockdown dramatically suppressed Hsp70 induction after heat-shock stress (**Fig. 5a,b**). The deficient Hsp70 synthesis is specific to MRPL18 because knocking down other mitochondrial ribosomal proteins did not influence the cytosolic stress response at all (**Supplementary Fig. 7a,b**). These data collectively highlight MRPL18(cyto) as a critical mediator of the cytosolic stress response.

MRPL18(cyto) promotes ribosome engagement on stress mRNAs

The participation of MRPL18(cyto) in Hsp70 synthesis suggests that a specialized ribosome might be required for mRNA translation under stress conditions. MRPL18 is a homolog of cytoplasmic RPL5, according to sequence alignment. Much like RPL5, MRPL18 binds to 5S rRNA and is believed to import the 5S rRNA into mitochondria[29]. An *in vitro* RNA binding assay confirmed that 5S rRNA strongly associates with recombinant MRPL18(ATG) but not GFP (**Supplementary Fig. 7d,e**). However, we found little evidence indicating that MRPL18 replaces RPL5 in binding to the 80S ribosome (**Fig. 3**). In fact, RPL5 knockdown also reduced Hsp70 synthesis after heat-shock stress (**Supplementary Fig. 7c**). Notably, MRPL18 does not seem to interact with separated 40S or 60S subunits (**Supplementary Fig. 7f**). It is thus likely that MRPL18(cyto) serves as an extra RP in binding to the

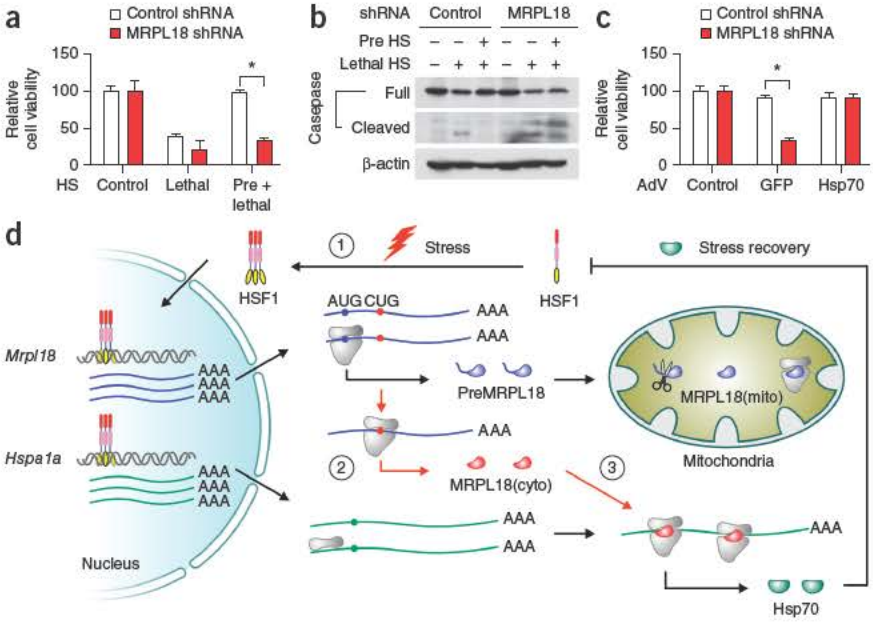

Figure 7 Cytosolic MRPL18 is essential for induced thermal tolerance. (**a**) Thermal tolerance analysis of MEFs lacking MRPL18. MEFs transfected with shRNA targeting MRPL18 or control shRNA targeting scrambled sequences were primed with mild heat shock (43 °C for 30 min) and allowed to recover at 37 °C for 5 h (pre). Severe heat shock (45 °C for 1 h; lethal) was then applied before the cell viability assay. Error bars, s.e.m. ($n = 4$ cell cultures, $^*P < 0.01$ by two-tailed Student's t test). Control, no heat shock. (**b**) Examination of apoptotic markers in MEF cells as in **a** by immunoblotting with the indicated antibodies. (**c**) Thermal tolerance assays of MEFs after reintroduction of Hsp70. MEFs as in **a** were infected with recombinant adenoviruses (AdV) encoding GFP or Hsp70 before thermal tolerance analysis. Error bars, s.e.m. ($n = 3$ cell cultures, $^*P < 0.01$ by two-tailed Student's t test). Control, uninfected cells. (**d**) A model for MRPL18 in translational control during stress conditions. Stress conditions such as heat shock trigger trimerization and activation of HSF1 (1), which turns on genes including *Mrpl18* and *Hspa1a*. In nonstressed cells, MRPL18 translation is initiated from the annotated AUG, generating MRPL18 containing a mitochondria localization signal (blue). In stressed cells, MRPL18 undergoes alternative translation from the downstream CUG start codon, which results in a cytoplasmic isoform of MRPL18 (red) (2). MRPL18(cyto) incorporates into the 80S ribosome complex, facilitating the engagement of mRNAs highly expressed under stress, such as *Hspa1a* (green) (3). The efficient synthesis of heat-shock proteins contributes to stress recovery. Original blot images are in **Supplementary Data Set 1**.

80S ribosome. 5S rRNA forms the central protuberance of the large ribosomal subunit[30]. This region is of particular importance because it nears the place where the ribosomal large and small subunits, the decoded mRNA and the peptidyl tRNA all come together. We postulate that the presence of an extra RP promotes 80S ribosome engagement on mRNAs during stress conditions. To test this hypothesis, we examined the distribution of Hsp70 mRNA in the polysome fractions of stressed MEF cells with or without MRPL18 knockdown (**Fig. 6d**). With comparable total mRNA levels, the Hsp70 transcript showed much less enrichment in the polysomes of MEFs lacking MRPL18. In contrast, control β-actin mRNA exhibited only minor reduction in the polysomes of these cells, presumably because of the delayed stress recovery as a result of impaired Hsp70 synthesis. Indeed, MEFs lacking MRPL18 showed less polysome formation during stress recovery (**Fig. 6d**).

MRPL18 is essential for induced thermotolerance

Because of the essential role of chaperone molecules in cell survival, we predict that cells lacking MRPL18 should have attenuated thermotolerance. Induced thermotolerance allows cells to survive a normally lethal temperature if they are first conditioned at a milder temperature. Without preconditioning, MEFs with or without MRPL18 knockdown were equally susceptible to severe heat stress at 45 °C for 1 h (**Fig. 7a**). Preexposure at 43 °C for 30 min resulted in a nearly complete protection of control MEF cells from severe heat stress. However, we no longer observed the induced thermotolerance in MEFs with MRPL18 knockdown. As expected, the reduced cell viability in the absence of MRPL18 was largely due to increased apoptosis (**Fig. 7b**). In agreement with the suppressed chaperone biosynthesis in cells lacking MRPL18, reintroduction of Hsp70 by recombinant adenoviruses completely restored the thermotolerance (**Fig. 7c**). Given the broad range of chaperone function in cell physiology, it would be of much interest to investigate possible protective roles of MRPL18 against cellular stressors beyond heat shock.

DISCUSSION

Cells in nearly all living organisms respond to heat-shock stress by marked transcriptional alterations and rapid translational reprogramming[5]. Despite severe inhibition of the translation machinery under stress conditions, efficient synthesis of stress proteins persists by a mechanism that has not been completely understood. Here, we uncovered a molecular mechanism underlying the active translation of mRNAs highly expressed during stress. We show that heat-shock stress triggers a previously unrecognized alternative translation of MRPL18, which generates a cytoplasmic isoform of the mitochondrial ribosomal protein. Remarkably, the cytoplasmic version of MRPL18 incorporates into the 80S ribosome complex in a stress-dependent manner. The stress-induced formation of specialized ribosomes, together with the cap-independent translation initiation mechanism, ensures efficient translation of mRNAs under nonfavorable conditions (**Fig. 7d**). Our results thus provide a new paradigm for translational regulation under stress conditions, which involves ribosome specialization after an initial alternative translation event.

A growing body of evidence has suggested that ribosome heterogeneity prevails across species, under different developmental stages and in various tissues[31,32]. Variation in ribosome composition, in both rRNA and RPs, provides a regulatory mechanism to the translation machinery. A clear example is illustrated in *Escherichia coli*, in which the stress-induced endonuclease MazF cleaves the 16S rRNA and removes the anti–Shine-Dalgarno sequence[33]. The resultant 'stress ribosome' selectively translates the leaderless mRNAs, a group of transcripts also generated by MazF. In eukaryotes, certain RPs have been found to control transcript selectivity during translation. For example, RPL38 is required for translation of homeobox mRNAs[34], whereas RPL40 appears to control translation of vesicular stomatitis virus mRNAs[35]. In this report, we discovered in mammalian cells an unusual mechanism that allows HSP mRNA translation to escape from the shutoff of global protein synthesis. Instead of altering the rRNA structure, the mammalian stress ribosome uses an extra RP that functions in mitochondria at basal state. MRPL18(cyto) incorporation may alter ribosome conformation and/or stabilize ribosome engagement on mRNAs that are highly expressed under stress conditions. Alternatively, the presence of MRPL18(cyto) may cause recruitment of additional factors facilitating initiation and elongation. In any case, stress-induced ribosome heterogeneity permits translational reprogramming without rebuilding the entire translational machinery.

Another interesting phenomenon revealed by our data is the functional connection between mitochondrial and cytoplasmic ribosomes. The 55S mitochondrial ribosome differs substantially from the 80S ribosome in eukaryotic cytoplasm and the 70S ribosome in prokaryotes. In mammalian cells, the mitochondrial ribosome complex has a higher content of protein than rRNA components[14,36]. Although many MRPs are distinctive and evolving rapidly, MRPL18 has a close homolog in *E. coli*. Unlike many other RPs, MRPL18 has apparently evolved to become a stress-inducible gene in mammals. The possession of an alternative translation feature further renders MRPL18 a critical regulator of the stress response. We conclude that MRPL18 actively participates in stress adaptation by potentiating the cellular translation machinery to achieve a robust cytosolic stress response.

METHODS

Methods and any associated references are available in the online version of the paper.

Note: Any Supplementary Information and Source Data files are available in the online version of the paper.

ACKNOWLEDGMENTS

We thank J.W. Yewdell and T. Fox for critical reading of the manuscript. We also thank I. Benjamin (University of Utah) for providing *Hsf1*$^{+/+}$ and *Hsf1*$^{-/-}$ MEFs, R. Kaufman (Sanford Burnham Medical Research Institute) for eIF2α (S/S) and eIF2α (A/A) MEFs, and T. Wandless (Stanford) for plasmids encoding the FKBP destabilizing domain. This work was supported in part by US National Institutes of Health training grants to R.A.C. and C.S.C. B.L. was supported as a recipient of the Genomics Scholar's Award from the Center for Vertebrate Genomics at Cornell. This work was primarily supported by grants to S.-B.Q. from the US National Institutes of Health (DP2 OD006449 and R01AG042400), the Ellison Medical Foundation (AG-NS-0605-09) and the US Department of Defense (W81XWH-14-1-0068).

AUTHOR CONTRIBUTIONS

X.Z. and S.-B.Q. conceived the original idea and designed the experiments. X.Z. performed the majority of the experiments. X.G. conducted luciferase reporter assays. R.A.C. assisted in polysome gradient analysis. C.S.C. conducted ^{35}S metabolic labeling assays. B.L. assisted in data interpretation. S.-B.Q. wrote the manuscript, and all authors edited the manuscript.

COMPETING FINANCIAL INTERESTS

The authors declare no competing financial interests.

1. Holcik, M. & Sonenberg, N. Translational control in stress and apoptosis. *Nat. Rev. Mol. Cell Biol.* **6**, 318–327 (2005).
2. Spriggs, K.A., Bushell, M. & Willis, A.E. Translational regulation of gene expression during conditions of cell stress. *Mol. Cell* **40**, 228–237 (2010).
3. Jackson, R.J., Hellen, C.U. & Pestova, T.V. The mechanism of eukaryotic translation initiation and principles of its regulation. *Nat. Rev. Mol. Cell Biol.* **11**, 113–127 (2010).

4. Panniers, R. Translational control during heat shock. *Biochimie* **76**, 737–747 (1994).
5. Richter, K., Haslbeck, M. & Buchner, J. The heat shock response: life on the verge of death. *Mol. Cell* **40**, 253–266 (2010).
6. Morimoto, R.I. Regulation of the heat shock transcriptional response: cross talk between a family of heat shock factors, molecular chaperones, and negative regulators. *Genes Dev.* **12**, 3788–3796 (1998).
7. Anckar, J. & Sistonen, L. Regulation of HSF1 function in the heat stress response: implications in aging and disease. *Annu. Rev. Biochem.* **80**, 1089–1115 (2011).
8. McGarry, T.J. & Lindquist, S. The preferential translation of *Drosophila* hsp70 mRNA requires sequences in the untranslated leader. *Cell* **42**, 903–911 (1985).
9. Klemenz, R., Hultmark, D. & Gehring, W.J. Selective translation of heat shock mRNA in *Drosophila melanogaster* depends on sequence information in the leader. *EMBO J.* **4**, 2053–2060 (1985).
10. Rubtsova, M.P. *et al.* Distinctive properties of the 5′-untranslated region of human hsp70 mRNA. *J. Biol. Chem.* **278**, 22350–22356 (2003).
11. Sun, J., Conn, C.S., Han, Y., Yeung, V. & Qian, S.B. PI3K-mTORC1 attenuates stress response by inhibiting cap-independent Hsp70 translation. *J. Biol. Chem.* **286**, 6791–6800 (2011).
12. Moore, P.B. How should we think about the ribosome? *Annu Rev Biophys* **41**, 1–19 (2012).
13. Kressler, D., Hurt, E. & Bassler, J. Driving ribosome assembly. *Biochim. Biophys. Acta* **1803**, 673–683 (2010).
14. Christian, B.E. & Spremulli, L.L. Mechanism of protein biosynthesis in mammalian mitochondria. *Biochim. Biophys. Acta* **1819**, 1035–1054 (2012).
15. Lee, S., Liu, B., Huang, S.X., Shen, B. & Qian, S.B. Global mapping of translation initiation sites in mammalian cells at single-nucleotide resolution. *Proc. Natl. Acad. Sci. USA* **109**, E2424–E2432 (2012).
16. Trinklein, N.D., Murray, J.I., Hartman, S.J., Botstein, D. & Myers, R.M. The role of heat shock transcription factor 1 in the genome-wide regulation of the mammalian heat shock response. *Mol. Biol. Cell* **15**, 1254–1261 (2004).
17. Mendillo, M.L. *et al.* HSF1 drives a transcriptional program distinct from heat shock to support highly malignant human cancers. *Cell* **150**, 549–562 (2012).
18. Qian, S.B., McDonough, H., Boellmann, F., Cyr, D.M. & Patterson, C. CHIP-mediated stress recovery by sequential ubiquitination of substrates and Hsp70. *Nature* **440**, 551–555 (2006).
19. Margeot, A. *et al.* In *Saccharomyces cerevisiae*, ATP2 mRNA sorting to the vicinity of mitochondria is essential for respiratory function. *EMBO J.* **21**, 6893–6904 (2002).
20. Banaszynski, L.A., Chen, L.C., Maynard-Smith, L.A., Ooi, A.G. & Wandless, T.J. A rapid, reversible, and tunable method to regulate protein function in living cells using synthetic small molecules. *Cell* **126**, 995–1004 (2006).
21. Sonenberg, N. & Hinnebusch, A.G. New modes of translational control in development, behavior, and disease. *Mol. Cell* **28**, 721–729 (2007).
22. Harding, H.P., Calfon, M., Urano, F., Novoa, I. & Ron, D. Transcriptional and translational control in the mammalian unfolded protein response. *Annu. Rev. Cell Dev. Biol.* **18**, 575–599 (2002).
23. Vattem, K.M. & Wek, R.C. Reinitiation involving upstream ORFs regulates ATF4 mRNA translation in mammalian cells. *Proc. Natl. Acad. Sci. USA* **101**, 11269–11274 (2004).
24. Wek, R.C., Jiang, H.Y. & Anthony, T.G. Coping with stress: eIF2 kinases and translational control. *Biochem. Soc. Trans.* **34**, 7–11 (2006).
25. Duncan, R.F. & Hershey, J.W. Protein synthesis and protein phosphorylation during heat stress, recovery, and adaptation. *J. Cell Biol.* **109**, 1467–1481 (1989).
26. Scheuner, D. *et al.* Translational control is required for the unfolded protein response and *in vivo* glucose homeostasis. *Mol. Cell* **7**, 1165–1176 (2001).
27. Yamanashi, Y. *et al.* The yes-related cellular gene lyn encodes a possible tyrosine kinase similar to p56lck. *Mol. Cell. Biol.* **7**, 237–243 (1987).
28. Lin, R.Z., Hu, Z.W., Chin, J.H. & Hoffman, B.B. Heat shock activates c-Src tyrosine kinases and phosphatidylinositol 3-kinase in NIH3T3 fibroblasts. *J. Biol. Chem.* **272**, 31196–31202 (1997).
29. Smirnov, A., Entelis, N., Martin, R.P. & Tarassov, I. Biological significance of 5S rRNA import into human mitochondria: role of ribosomal protein MRP-L18. *Genes Dev.* **25**, 1289–1305 (2011).
30. Szymański, M., Barciszewska, M.Z., Erdmann, V.A. & Barciszewski, J. 5 S rRNA: structure and interactions. *Biochem. J.* **371**, 641–651 (2003).
31. Xue, S. & Barna, M. Specialized ribosomes: a new frontier in gene regulation and organismal biology. *Nat. Rev. Mol. Cell Biol.* **13**, 355–369 (2012).
32. Gilbert, W.V. Functional specialization of ribosomes? *Trends Biochem. Sci.* **36**, 127–132 (2011).
33. Vesper, O. *et al.* Selective translation of leaderless mRNAs by specialized ribosomes generated by MazF in *Escherichia coli*. *Cell* **147**, 147–157 (2011).
34. Kondrashov, N. *et al.* Ribosome-mediated specificity in Hox mRNA translation and vertebrate tissue patterning. *Cell* **145**, 383–397 (2011).
35. Lee, A.S., Burdeinick-Kerr, R. & Whelan, S.P. A ribosome-specialized translation initiation pathway is required for cap-dependent translation of vesicular stomatitis virus mRNAs. *Proc. Natl. Acad. Sci. USA* **110**, 324–329 (2013).
36. O'Brien, T.W. Properties of human mitochondrial ribosomes. *IUBMB Life* **55**, 505–513 (2003).